

Article

# Prediction of Wind Environment and Indoor/Outdoor Relationships for PM<sub>2.5</sub> in Different Building–Tree Grouping Patterns

Bo Hong<sup>1</sup>, Hongqiao Qin<sup>1</sup> and Borong Lin<sup>2,\*</sup>

<sup>1</sup> College of Landscape Architecture & Arts, Northwest A&F University, Yangling 712100, China; hongbo@nwsuaf.edu.cn (B.H.); qinhq88@163.com (H.Q.)

<sup>2</sup> Department of Building Science, School of Architecture, Tsinghua University, Beijing 100084, China

\* Correspondence: linbr@tsinghua.edu.cn; Tel.: +86-010-6278-5691

Received: 26 October 2017; Accepted: 22 January 2018; Published: 24 January 2018

**Abstract:** Airflow behavior and indoor/outdoor PM<sub>2.5</sub> dispersion in different building–tree grouping patterns depend significantly on the building–tree layouts and orientation towards the prevailing wind. By using a standard  $k$ - $\epsilon$  model and a revised generalized drift flux model, this study evaluated airflow fields and indoor/outdoor relationships for PM<sub>2.5</sub> resulting from partly wind-induced natural ventilation in four hypothetical building–tree grouping patterns. Results showed that: (1) Patterns provide a variety of natural ventilation potential that relies on the wind influence, and buildings that deflect wind on the windward facade and separate airflow on the leeward facade have better ventilation potential; (2) Patterns where buildings and trees form a central space and a windward opening side towards the prevailing wind offer the best ventilation conditions; (3) Under the assumption that transported pollution sources are diluted through the inlet, the aerodynamics and deposition effects of trees cause the lower floors of a multi-storey building to be exposed to lower PM<sub>2.5</sub> compared with upper floors, and lower indoor PM<sub>2.5</sub> values were found close to the tree canopy; (4) Wind pressure differences across each flat showed a poor correlation ( $R^2 = 0.059$ ), with indoor PM<sub>2.5</sub> concentrations; and (5) Patterns with the long facade of buildings and trees perpendicular to the prevailing wind have the lowest indoor PM<sub>2.5</sub> concentrations.

**Keywords:** wind environment; Natural Ventilation Potential (NVP); PM<sub>2.5</sub>; building–tree grouping patterns; Computational Fluid Dynamics (CFD)

## 1. Introduction

With the rapid development of urbanization, particulate matter (PM) pollution, especially types with an aerodynamic diameter of less than 2.5  $\mu\text{m}$  (PM<sub>2.5</sub>), has led to a dramatic decline in urban air quality. PM<sub>2.5</sub> pollution has been confirmed to have a close relationship with the human respiratory system, resulting in cardiopulmonary system damage and high incidences of cancer [1]. In addition, a nationally representative survey of communities, families, and individuals in China showed that air pollution reduced hedonic happiness and raised the rate of depression symptoms [2]. In built environments, outdoor-generated particles are major contributors to indoor pollution, without strong internal pollution sources [3–6]. Since most people spend approximately 85–90% of their time indoors, determining the relationships between outdoor particle sources and the corresponding indoor concentrations are especially significant when measuring particulate concentrations in occupied residences [7].

Natural ventilation is extensively used to provide better indoor air quality without using electricity [8]. Some knowledge of the relationships between wind velocity, wind direction, and ventilation characteristics is needed to ventilate naturally [9]. In addition to the types of natural vents, the outdoor

wind environment acts as a significant factor that affects the natural ventilation potential [10]. A comparison of Computational Fluid Dynamics (CFD) simulation results has been carried out to examine the accuracy of wind environment measurements around a single building and building complexes in urban areas [11]. Wind fields strongly depend on the building layout and prevailing wind, and staggered arrangements could provide a comfortable wind environment and sufficient natural ventilation potential with S–N and SE–NW wind directions [12,13]. Additionally, CFD simulations indicated that the outdoor wind environment relies on building geometry, spacing, grouping patterns, and orientation towards the prevailing wind [14–18]. Furthermore, the aerodynamic effects of trees on airflows have also attracted attention. The accuracy of the aerodynamic effects of trees has been examined for a pedestrian-level wind environment assessment [19]. The optimum arrangement of trees for creating a comfortable outdoor environment and sufficient natural ventilation was tested with numerical simulations and field experiments in a residential neighborhood [20–22]. The influence of different building–tree arrangements on natural ventilation potential and outdoor thermal comfort was investigated via a simulation platform for an outdoor thermal environment [23].

Considerable research has also examined the behavior of indoor/outdoor air pollutant dispersion in different types of buildings. The indoor/outdoor (I/O) ratio, penetration, and infiltration factors are considered the main factors expressing the connection between indoor and outdoor particle concentrations [24]. The measured data showed that indoor particles were highly correlated with outdoor particles, but negatively coordinated with wind velocity [25–28]. The infiltration rate was affected by wind velocity, but little by temperature [29,30]. A field investigation indicated that PM<sub>2.5</sub> and PM<sub>10</sub> were approximately equal when measured inside and outside of a building next to roads with high traffic emissions. The I/O ratio also differs whether building windows were open and closed [31]. Field experiments on indoor/outdoor and seasonal variations have indicated that particle concentrations are highest in winter due to low wind speed and high outdoor humidity compared with other seasons [32]. More pollutants from outdoors entered naturally ventilated rooms in winter than in other seasons [33].

Several numerical studies have also investigated indoor particle concentrations generated from outside pollutants [34]. Simulations have confirmed that particle deposition was mainly affected by the ventilation conditions, and that the deposition rate under displacement ventilation was lower than mixed ventilation, but the escaped particle mass is larger, and the average pollutants concentration is higher in the former than the latter [35]. In addition, a combined empirical and simulated method was used to appraise the effectiveness of deep bag and electrostatic filters to reduce PM. The results revealed that an air filter can significantly reduce the indoor PM, and particle dynamics and movement in office buildings under different ventilation were quantified [36]. However, few studies have examined the effect of trees on indoor and outdoor particle dispersion, and the study of indoor PM<sub>2.5</sub> removal by natural ventilation exerted by building–tree arrangements is one of fundamental and practical significances in the design stage.

Overall, many full-scale field experiments and simulation studies have illustrated that indoor particles originate largely outdoors, and that building ventilation has a significant influence on the particle diffusion process [25,37–40]. Some studies have illustrated airflow fields around different building grouping patterns [17], or various building–tree arrangements on airflows and outdoor particle dispersion [41]. Moreover, according to the Annual Report on Chinese Building Energy Conservation Development 2016, most residents in cold regions still opened the windows in the cold winter days for ventilation over 1 h accumulatively to reduce indoor CO<sub>2</sub> concentration, due to a lack of air conditioning systems [42]. Based on the monitored data, the probability of window opening would be randomly high or low over a short period during the winter in Beijing. For example, when outdoor PM<sub>2.5</sub> concentration was 245 µg/m<sup>3</sup> in Beijing during the monitoring periods, the corresponding probability of window opening was 100% [43]. This suggests that partly wind-driven natural ventilation in cold seasons could affect the indoor PM<sub>2.5</sub> dispersions. Under the circumstance of high PM<sub>2.5</sub> concentrations during the winter in Beijing, it may be possible to analyze the influence

of building–tree arrangements on indoor and outdoor relationships for PM<sub>2.5</sub> dispersion in winter resulting from partly wind-driven natural ventilation, to uncover optimal patterns that improve indoor air quality.

This study performed numerical simulations with CFD code, coupled with the standard  $k$ - $\epsilon$  model and the generalized drift flux model, to determine: (1) The effects of four building–tree grouping patterns on the outdoor wind environment and the indoor and outdoor relationships for PM<sub>2.5</sub> as a result of partly wind-induced natural ventilation in Beijing; (2) The relationship between the resulting wind pressure differences and indoor PM<sub>2.5</sub> concentrations; and (3) Which configuration can provide the best ventilation potential or provide the lowest indoor PM<sub>2.5</sub> concentrations.

## 2. Climate of Beijing

Beijing's climate is characterized as typical of a warm, continental, monsoon zone, with daily average temperatures in summer and winter of 26.5 °C and −3.8 °C, respectively. The daily relative humidity ranges from 56.6 to 74.1% in summer, and from 39.4 to 45.8% in winter. The prevailing winds are southerly and southeasterly in summer, and the average wind velocity reaches 2.0 m/s. Prevailing winds during the winter are northerly and northwesterly, with an average velocity of 2.6 m/s. Based on weekly data, the highest level of PM<sub>2.5</sub> pollution is between mid-November and December [44]. Data reported by the Beijing Meteorological Service indicated that the average wind velocity in November and December 2015 was 2.3 m/s, and the dominant wind directions were northerly, northwesterly, and westerly. The average temperature ranged from −0.5 °C to 5.4 °C, and relative humidity ranged from 45.4 to 55.6%. The average PM<sub>2.5</sub> during this time period was 134 µg/m<sup>3</sup> [45], which is almost four times higher than the World Health Organization's interim target-1 (IT-1) level. The annual mean concentration of IT-1 is 35 µg/m<sup>3</sup>, and this level is associated with approximately a 15% higher long-term mortality risk relative to the air quality guideline (AQG) level [46].

## 3. Simulation Case Descriptions

The airflow and PM<sub>2.5</sub> dispersion around the grouped buildings and trees are affected by several factors, including: building geometry, grouping patterns, orientation with respect to the prevailing wind, and tree-building distance. Based on Beijing's climate in November and December 2015, four common buildings configurations with a reference wind velocity of 2.3 m/s and two prevailing wind directions (northerly and westerly) were selected for testing.

The first configuration is two parallel rows of housing blocks. The second block contains a T-shaped central space that adopts a semi-open array architectural layout. The third is a staggered pattern with the buildings turned 90° to one another. The architectural layout of the fourth is known as a peripheral array in which each building block measures 30 m × 15 m × 18 m and rises six storeys. The building blocks are regarded as solid blocks with no wind permeability considered. The area of the target site is 6400 m<sup>2</sup> (80 m × 80 m), with coverage ratios of 71% to allow space for outdoor activity. Cypress (*Platycladus orientalis*) trees, with conical crown morphology, are planted along the building 2.5 m from the building base. The leaf area density of cypress is 2.3 m<sup>2</sup>/m<sup>3</sup>, and the deposition velocity for PM<sub>2.5</sub> is 0.0458 m/s [47]. The tree height, crown diameter, and clear bole height are 5 m, 3 m, and 2 m, respectively (Figure 1).

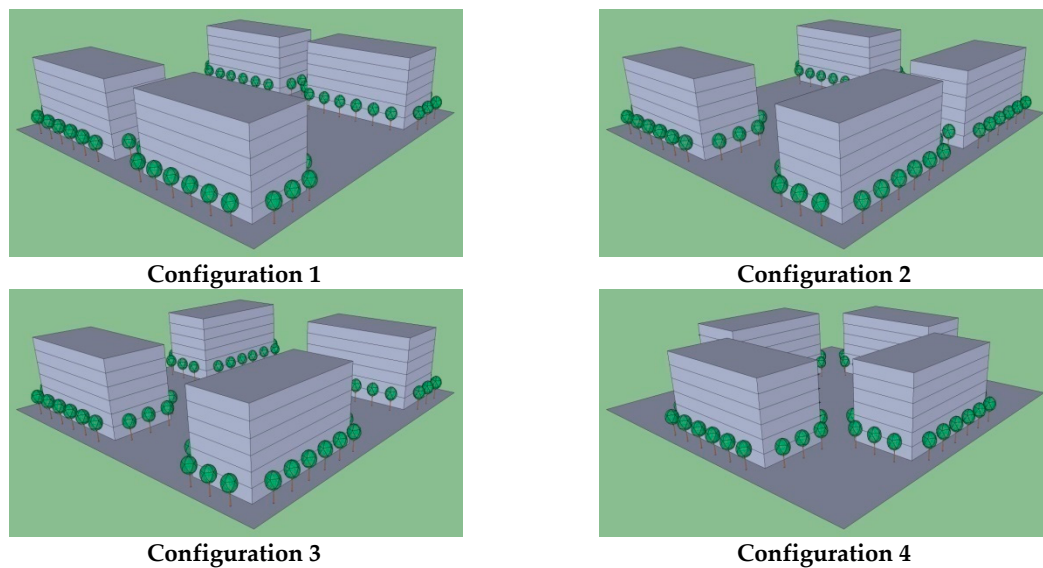


**Figure 1.** Illustration of building–tree grouping patterns modeled in this study. **Configuration 1** is the parallel rows; **Configuration 2** is the internal T; **Configuration 3** is staggered; **Configuration 4** is the peripheral array.

## 4. The CFD Code

### 4.1. Simulation Models

Parabolic Hyperbolic or Elliptic Numerical Integration Code Series (PHOENICS) was used in this study as a three-dimensional simulation tool, and the standard  $k$ - $\epsilon$  model was selected. The Semi-Implicit Method for Pressure-Linked Equations (SIMPLE) algorithm with the Quadratic Upstream Interpolation for Convective Kinematics (QUICK) discretization scheme is applied to all governing equations except the concentration equation [48], for which a Sharp and Monotonic Algorithm for Realistic Transport (SMART) scheme is adopted to avoid negative concentrations near sources. The simulation process was facilitated by the use of an i7 2.67 GHz processor, while, the PHOENICS 2009 program was used to process the solution.

In this model, vegetation is described as a porous medium with branches and trunk comprising the canopy. The influence of vegetation on the flow field was to decrease air velocity by exerting drag forces and pressure, and the canopy elements that reduced air velocity created additional turbulence levels [49]. The consequent effects of vegetation on turbulent flow fields were modeled, and drag forces were included in the momentum equations. Additional source terms were also included in transport equations for turbulent kinetic energy,  $k$ , and its dissipation rate,  $\epsilon$ . Turbulence production and accelerated turbulence dissipation within the canopy were accounted for by the additional turbulence source terms [50].

Flow resistance, which is generated by turbulent flow through the plant canopy, is represented by introducing the following sink term into the momentum equations:

$$S_{d,i} = -C_d \alpha(z) |U| u_i \quad (1)$$

where  $C_d$  is the drag coefficient,  $\alpha(z)$  is the leaf area density (LAD) ( $\text{m}^2/\text{m}^3$ ),  $z$  is the vertical space coordinate,  $|U|$  is the magnitude of the superficial velocity vector, and  $u_i$  is the superficial value of the Cartesian velocity in the direction  $i$  (m/s).

Vegetation density is characterized by the integral value of leaf area density. The integral value is determined by the leaf area index (LAI), which is defined by the following equation:

$$LAI = \int_0^h \alpha(z) dz \tag{2}$$

where  $h$  is the average height of the canopy.

The turbulent interactions between the plant canopy and airflow, including the following additional source terms in the transport equations for  $k$  and  $\epsilon$ , are described as:

$$S_k = C_d \alpha(z) (\beta_p |U|^3 - \beta_d |U|k) \tag{3}$$

$$S_\epsilon = C_d \alpha(z) (C_{4\epsilon} \beta_p |U|^3 \frac{\epsilon}{k} - C_{5\epsilon} \beta_d |U|\epsilon) \tag{4}$$

where the constant  $\beta_p$  is the fraction of mean-flow kinetic energy converted to wake-generated  $k$  by canopy drag, and  $\beta_d$  is the fraction of  $k$  dissipated by the Kolmogorov energy cascade short-circuiting. In this study, the constants  $\beta_p$  and  $\beta_d$ , and the closure constants  $C_{4\epsilon}$  and  $C_{5\epsilon}$  are given the values 1.0, 3.0, 1.5, and 1.5, respectively [51–53].

To model the particle dispersion procedure, the revised generalized drift flux model, which was modified from the Eulerian model by adding additional terms for particle absorption and the resuspension by trees, was used [54]. In the model, particles are treated as a continuum, and particle movements are assumed to not affect turbulence. The convective velocity of the particle phase is assumed to be the same as the airflow, which has been widely used in recent studies [55–57], and greatly reduced the complexity of the two-phase flow simulation. The model is expressed as follows:

$$\frac{\partial [(V_j + V_{slip,j})C]}{\partial x_j} = \frac{\partial}{\partial x_j} \left[ \epsilon_p \frac{\partial C}{\partial x_j} \right] + S_c - S_{sink} + S_{resuspension} \tag{5}$$

The additional terms  $S_{sink}$  and  $S_{resuspension}$  are calculated as:

$$S_{sink} = V_d \times C \times \alpha \tag{6}$$

$$S_{resuspension} = V_r \times C_{sink} \times \alpha \tag{7}$$

where  $V_j$  is the spatial mean fluid (air) velocity (m/s);  $V_{slip,j}$  is the gravitational settling velocities of particles in  $j$  direction (m/s);  $C$  is the inlet concentration ( $\mu\text{g}/\text{m}^3$ );  $\epsilon_p$  is the eddy diffusivity ( $\text{m}^2/\text{s}$ );  $S_c$  is the generated rate of the pollution source ( $\text{kg}/(\text{m}^3 \cdot \text{s})$ );  $S_{sink}$  is the mass of particles absorbed per unit vegetation volume per unit time ( $\mu\text{g}/\text{m}^3$ );  $S_{resuspension}$  is the secondary pollutants from foliage per unit vegetation volume per unit time ( $\mu\text{g}/\text{m}^3$ ) [58];  $V_d$  is the particle deposition velocity on plant foliage (m/s);  $V_r$  is the particle resuspension velocity from plant foliage (m/s);  $C_{sink}$  is the particle concentration deposited on plant foliage ( $\mu\text{g}/\text{m}^3$ ); and  $\alpha$  is LAD ( $\text{m}^2/\text{m}^3$ ).

#### 4.2. Model Validation

To validate models against the wind tunnel dataset issued by the Laboratory of Building and Environmental Aerodynamics at the Karlsruhe Institute of Technology (KIT) [59], models of street canyons with two rows of avenue trees were built and set according to the wind tunnel model represented. The height, width, and length of street canyons in the model were  $H$ ,  $2H$ , and  $10H$ , respectively.  $H$  is equal to 18 m. The tree canopy was 7.56 m wide ( $0.42H$ ), 12 m high ( $2/3H$ ), and 180 m ( $10H$ ) long. They were planted 5.22 m ( $0.29H$ ) away from street canyons. Traffic exhaust sources were placed in two rows along the street. Based on literature sources [60], the distance from inlet to windward building, from downwind building to outlet, and from buildings to both boundaries were set to  $5H$ ,  $20H$ , and  $9H$ , respectively. The height of the domain was  $11H$ . The grid in the target area consisted of elements with  $X_{min} = Y_{min} = Z_{min} = 0.028H$ , and grid independence evaluated by the grid

convergence index (GCI) showed that the GCI value was 2.53% (less than 5%), demonstrating that the used grid arrangement was fine enough [61]. Boundary conditions were set according to wind tunnel experiments [62].

Since the models should be verified against experimental data, the simulated parameters should be selected considering the Concentration Data of Street Canyons (CODASC) wind tunnel experiments. In the wind tunnel tests, trees were modeled with porous media with different porosities, and the deposition effect was not considered. The different porosity was described by the pressure loss coefficient  $C_x$ . The  $C_x$  in the CODASC wind tunnel models were 80 and 200  $m^{-1}$  with trees, representing 0.53 and 1.33  $m^{-1}$  at a scale of 1:150, respectively. Correspondingly, simulation models set additional terms ( $S_{sink}$  and  $S_{resuspension}$ ) to zero, and the  $C_x = 1.33 m^{-1}$  was selected to compare the simulated data with scenarios in CODASC wind tunnel experiments. To obtain comparable results, vertical concentrations 0.75 m from both walls in the street canyon were measured in the simulation. Figure 2 shows the scatter plots of  $C_x = 1.33 m^{-1}$ . It can be seen that there were strong correlations between the simulated and wind tunnel data ( $R^2 = 0.926$  in wall A and  $R^2 = 0.991$  in wall B). According to Hanna and Chang [63], a set of acceptance criteria:  $-0.3 < FB < 0.3$ ,  $NMSE < 1.5$ ,  $0.5 < FAC2 < 2$ ,  $NAD < 0.3$ , and  $R > 0.8$  was recommended for further analysis. All of the metrics are within acceptance ranges, indicating the numerical models were suitable for predicting the airflow and pollutant dispersion within the street canyon (Table 1).

Additionally, the implemented models have been validated by the author in a previous study that compared simulated and measured data from a residential district in Beijing [64]. Parameters including wind velocity and  $PM_{2.5}$  concentrations were compared, and the results showed high correlations ( $R^2 = 0.910$  for wind velocity, and  $R^2 = 0.906$  for  $PM_{2.5}$  concentrations), indicating that the models accurately represented the real environment.

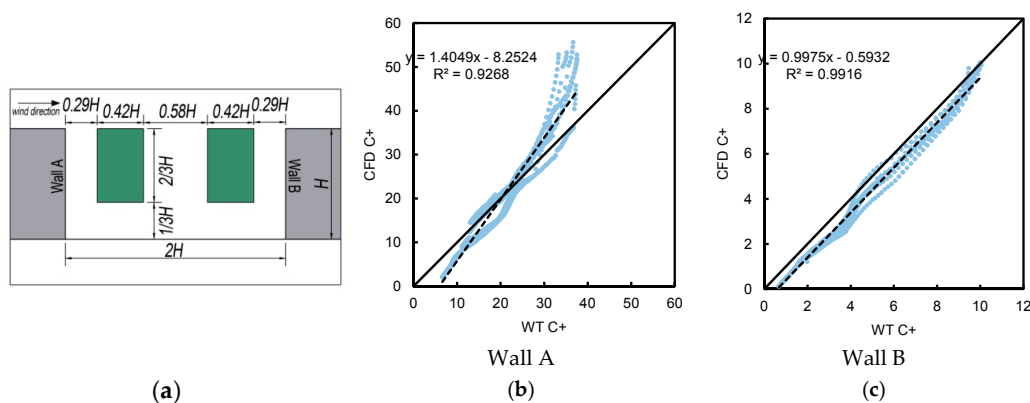


**Figure 2.** Model lateral view and dimensions (Wall A is the leeward wall of the upwind building, wall B is the windward wall of the downwind building) (a), and comparisons between normalized concentration results in wind tunnel experiments (WT  $C^+$ ) and simulations (CFD  $C^+$ ) (b,c).  $C^+$  is normalized by  $C^+ = C_m H U_H / Q_l$  ( $C_m$  is measured concentration,  $H$  is building height (m),  $U_H$  is wind velocity at height  $H$  (m/s), and  $Q_l$  is the emission rate of a line source ( $m^2/s$ )). Dashed lines are linear fits, with linear equations and  $R^2$ -values alongside. Diagonals depict perfect matches.

**Table 1.** Mean concentration results and statistical analysis metrics for  $C_x = 1.33 m^{-1}$ .

Wall	Mean Concentration*			Statistical Analysis Metrics				
	WT $C^+$	CFD $C^+$	RD	FB	NMSE	FAC2	NAD	R
A	20.77	20.92	6.6%	-0.007	0.052	1.008	0.083	0.961
B	3.90	3.30	-15.4%	0.1674	0.033	0.846	0.084	0.994

\* RD is relative difference; FB is fractional bias; NMSE is normalized mean square error; FAC2 is the fraction of predictions within a factor of two of observations; NAD is normalized absolute difference; and R is relation coefficient.

### 4.3. Domain Size and Grid Independence Testing

To match published recommendations [14,48], the distance of the computational domain inlet to the target area was set to  $5H$ , and the outlet boundary was set  $15H$  distant from the target area. A symmetry condition was imposed at the left and right lateral sides of  $5H$ , and the height from the ground to the top plane was set to  $11H$  (Figure 3). A mesh size was set using a horizontal and vertical hierarchy to ensure reasonable file sizes and computing time. To achieve this, a tetrahedral meshing scheme was used. Based on European Cooperation in Science & Technology (COST) recommendations, more than 10 cells per cube root of the building volume must be set as the mesh size [48]. Considering the inputs of this study, a mesh size larger than  $1.5 \times 10^6$  has been maintained to ensure a higher resolution, and three different grid sizes were tested by grid convergence index (GCI) to validate the grid independency of the numerical simulation, following the procedures proposed by Hefny and Ooka [65] (Table 2). Tests indicated that the GCI (u) for coarse and fine meshes differed by 2.72%, whereas those for fine and finest mesh differed by 2.61%. The GCIs (u) differences were all less than 5%, which indicated that fine meshes were sufficient. Element dimensions were selected as  $X_{min} = Y_{min} = Z_{min} = 0.05H$  to assure rational file sizes and save computation time.

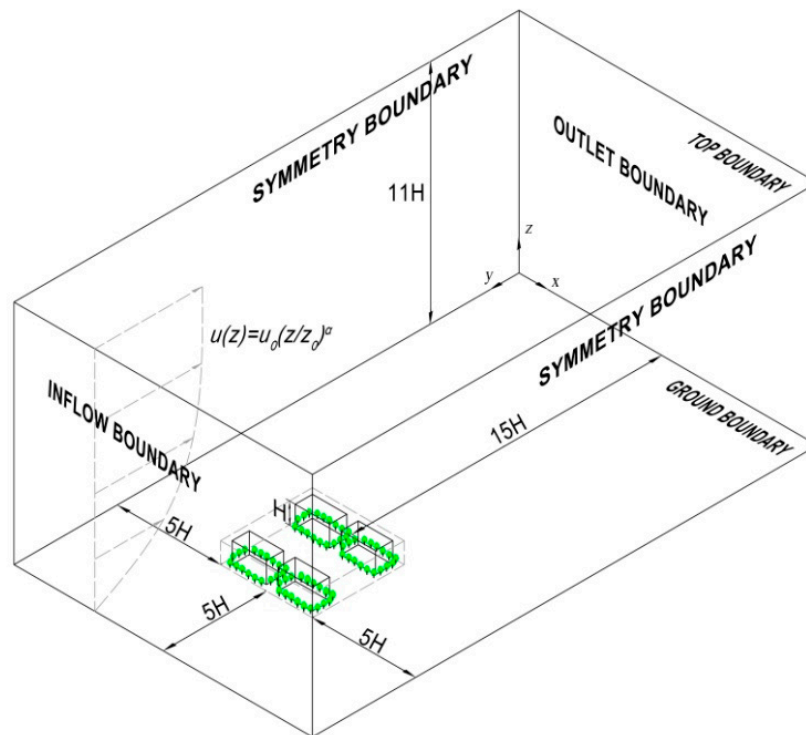


Figure 3. The computational domain.

Table 2. Different grid size for the computational domain.

Mesh	Minimum Grid Dimension	Total Cellnumber
coarse mesh	$X_{min} = Y_{min} = Z_{min} = 0.1H$	1,566,234
fine mesh	$X_{min} = Y_{min} = Z_{min} = 0.05H$	3,001,458
finest mesh	$X_{min} = Y_{min} = Z_{min} = 0.02H$	5,863,544

### 4.4. Boundary Conditions and Turbulence Model

The boundary conditions implemented in this study were simply velocity inlet and outflow. As no internal pollution sources in the target area was assumed,  $PM_{2.5}$  sources were transported by wind

from outside of the target area [64]. Thus, the source of PM<sub>2.5</sub> was added through the inlet, and the concentration was evenly distributed throughout the entire inflow boundary. The gradient wind was set as the velocity inlet boundary, and expressed as:

$$u(z) = u_0(z/z_0)^\alpha \quad (8)$$

where  $u(z)$  is the horizontal air velocity at the height  $z$ ; and  $u_0$  is the horizontal air velocity at a reference height of  $z_0$ . In the model,  $u_0 = 2.3$  m/s,  $z = 1.5$  m, and  $z_0 = 10$  m.  $\alpha$  is set to 0.25 [66].

To model the outflow boundary, a fixed pressure and zero gradients were specified. The lateral planes were regarded as symmetry boundaries. For the ground boundary, a fully rough wall function with a surface roughness of 0.495 m (0.0275 $H$ ) was implemented. Moreover, the constant horizontal velocity and turbulent kinetic energy were fixed for the top boundary according to the inflow profiles.

The turbulent kinetic energy,  $k$  (m<sup>2</sup>/s<sup>2</sup>), and its dissipation rate,  $\varepsilon$  (m<sup>2</sup>/s<sup>3</sup>), were determined as follows:

$$k = \frac{u_*^2}{\sqrt{C_\mu}} \left(1 - \frac{z}{\delta}\right) \quad (9)$$

$$\varepsilon = \frac{u_*^3}{kz} \left(1 - \frac{z}{\delta}\right) \quad (10)$$

where  $u_*$  is the friction velocity, which is set as 0.52 m/s,  $\delta$  is the boundary layer depth, and  $k$  is the von Kàrmàn constant, which is set as 0.4. The constant  $C_\mu$  is set as 0.09.

There are several specification methods for the turbulence parameters, including turbulence intensity and length scale, which can be calculated independently from the transport equations. Based on the Reynolds number of the case, the turbulence intensity is determined to be 10%, and the length scale simply equals 0.06 $l$ , where  $l$  is the inlet height in this study.

#### 4.5. Convergence Criteria

Based on the recommendation of COST Action 732 [48], a convergence of scaled residuals down to  $10^{-5}$  was adopted as criteria to examine the results with the main output parameters monitored. In this study, the average wind pressure on building facades, and airflow velocity at the pedestrian level (1.5 m height), were selected for soughting. These results were monitored in different convergence criteria, starting with larger residuals convergence criteria  $10^{-3}$  up to  $10^{-6}$ . There was no significant difference in results in the case of using  $10^{-6}$  convergence criteria compared to  $10^{-5}$ , indicating that the solution converged.

#### 4.6. Simulation Target

Wind-induced ventilation depends strongly on the pressure distribution on building facades, and it is significantly affected by the upstream building characteristics and the prevailing wind [67]. Wind pressure is the main natural ventilation driving force in Beijing. It is normally positive on the windward facades, but negative on the roof and leeward facade, due to boundary layer separation occurring by a building's edges. Based on Bernoulli's principle, the wind pressure is defined by:

$$P_w = 0.5K\rho V^2 \quad (11)$$

where  $P_w$  is the wind pressure (Pa);  $K$  is the static pressure coefficient;  $\rho$  is the reference air density (Kg/m<sup>3</sup>); and  $V$  is the time-mean wind speed at datum level (m/s).

In this study, each building was six storeys high, and each storey was divided into four flats ( $a$ ,  $b$ ,  $c$ , and  $d$ ). The wind pressure differences across flat facades were calculated, and the natural ventilation potential across each flat was evaluated by the resulting average wind pressure difference across each flat. These were achieved by the following procedures for each case:

- (1) Average wind pressure of each building façade was recorded.



- (2) Pressure differences across flats *a* to *d* in each building were computed (Tables 3–6).
- (3) Contours of wind velocity and streamlines at the pedestrian level, and contours of wind velocity and streamlines in sections *A-A'* and *B-B'* were also presented for better understanding the surrounding wind environment.

The indoor PM<sub>2.5</sub> concentration can be calculated as:

$$C_{indoor} = A * \left( \frac{U_i}{\exp \ln(U_i)} \right)^B * \left( \frac{RH_i}{\exp \ln(RH_i)} \right)^C * C_{outdoor} \quad (12)$$

where  $C_{indoor}$  and  $C_{outdoor}$  are the mean concentrations indoors and outdoors; and  $U_i$  and  $RH_i$  are the outdoor wind velocity (m/s) and relative humidity (%) under the steady state *i*, respectively. *A* is the permeability coefficient of an exterior window crack. *B* and *C* represent the correction coefficients for outdoor wind velocity and relative humidity. Based on a previous study, the factors *A*, *B*, and *C* are set as 0.5719, −0.1825, and 0.1622, respectively, given weather conditions in Beijing [38]. Equation (12) has been validated by a monthly measured data in February 2014 in Beijing, and the predicted indoor PM<sub>2.5</sub> agreed well with the monitored indoor data ( $R^2 = 0.95$ ) [38]. Hence, this equation proved to be an effective and feasible mathematical model to predict indoor PM<sub>2.5</sub> in a naturally ventilated building with windows closed.

To achieve the prediction of outdoor and indoor PM<sub>2.5</sub> concentrations, the following procedures were implemented for each examined case:

- (1) Outdoor vertical PM<sub>2.5</sub> concentrations were measured 0.5 m from the building facade. This was done for each of the four buildings.
- (2) Indoor concentrations across flats *a* to *d* in each building can be computed by Equation (12), as presented in Tables 7–10.
- (3) Contours of pedestrian level PM<sub>2.5</sub> concentrations, and PM<sub>2.5</sub> dispersion in vertical level were also presented to understand the vertical PM<sub>2.5</sub> concentrations (Figures 8–11).

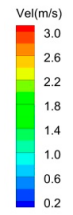
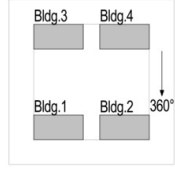
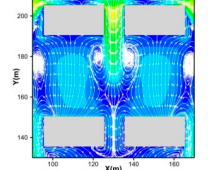
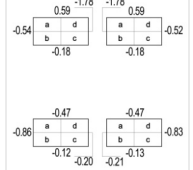
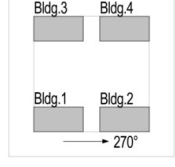
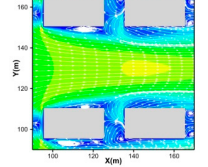
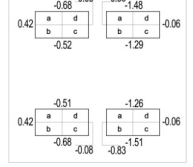
## 5. Results and Discussion

### 5.1. Analysis of Outdoor Wind Environment

#### 5.1.1. Configuration 1

The velocity contours and streamline distributions at the pedestrian level ( $Z = 1.5$  m), average wind pressure on facades, and wind pressure difference across flats in configuration 1 are presented in Table 3. In the 360° wind direction scenario, the outdoor airflow largely passed through the narrow space between two gable walls where the greatest wind speed occurred. Velocities suddenly increase at the leading sharp edge. The central space between two rows generated large vortexes and significant reversed-airflows. Vortexes at the two flanks were stronger than in the center. Due to the shading of windward buildings, the central space experienced low airflow movement. Meanwhile, streamlines converged at the space between two gables of leeward buildings, and the velocity increased in the convergence region. Wind speed decreased noticeably within trees, and the minimum speed occurred at the point where the trees were planted and vortexes arose (Figure 4a). In the 270° wind direction scenario, the airflow crossed over simulation fields easily from short facades without impediment. It appeared that the high wind speed in the wind corridor and the windward sharp edge had a rapidly increasing velocity. Vortexes arose mainly within trees with decreasing wind speed, and the minimum velocity occurred where the trees were planted. In addition, the 270° direction had more vortexes that were smaller than with north wind scenarios, and exerted more reversed airflows (Figure 4b).

**Table 3.** Results of configuration 1 showing velocity contours and streamlines around blocks at 1.5 m height (m/s), average wind pressure on facades,  $P_{av.}$  (Pa), and pressure differences across each flat,  $dP$ , (Pa).

V	Case	V Contours at 1.5 m	$P_{av.}$ (Pa)	$dP$ across Flats a to d (Pa)				
				Block No.				
				Bldg.1	Bldg.2	Bldg.3	Bldg.4	
				Block No.				
				Bldg.1 Bldg.2 Bldg.3 Bldg.4				
				a	-0.39	0.26	1.13	2.37
				b	0.74	0.08	-0.37	-1.60
c	0.08	0.70	-1.16	-0.34				
d	0.27	-0.36	2.38	1.10				
			Block No.					
			Bldg.1 Bldg.2 Bldg.3 Bldg.4					
			a	0.93	-0.43	1.10	-0.65	
			b	1.11	-0.68	0.95	-0.45	
c	-0.61	1.45	-0.45	1.23				
d	-0.43	1.19	-0.60	1.42				

An analysis of the wind pressure difference at 360° showed that the absolute values of windward building (Buildings 3 and 4) were higher than leeward buildings (Buildings 1 and 2), indicating the front blocks have better ventilation potential. Table 3 shows that Flats *a*, *b*, *c* and *d* of Building 3 are respectively equivalent to Flats *d*, *c*, *b*, and *a* of Building 4. Meanwhile, Buildings 1 and 2 perform the same corresponding relationship, and their corresponding flats have the same wind pressure difference. Thus, the resulting average wind pressure difference of Buildings 1 and 3 should be analyzed in this scenario. An analysis of Building 1 showed that the wind pressure difference for Flat *b* increased with building height, while Flat *c* had poor ventilation potential because of a small wind pressure difference (0.08 Pa). There is a higher negative pressure difference for the upper storey of Flats *a* and *d*. Wind pressure differences in Building 3 show those airflows through the building from the windward to leeward flats. In general, Flats *c* and *d* have better potential ventilation compared with Flats *a* and *b*. In the 270° wind direction scenario, the pressure differences among the buildings were relatively uniform, which was due to the airflow pattern that traveled from a wide space with few obstacles created by two parallel buildings exerting similar airflow surrounded by leeward and windward buildings. Meanwhile, wind pressure differences for leeward buildings are slightly higher than windward buildings. For this situation, the pressure differences of Buildings 1 and 2 are telling. An analysis of Building 1 showed that the absolute values for Flats *a* and *b* were higher than those of Flats *c* and *d*. An analysis of Building 2 showed that wind pressure differences were always positive and increased with building height for Flats *c* and *d*, with values of 1.45 and 1.19 Pa, respectively. The results from all of the buildings indicated that the highest absolute values appeared at the top storey, and the higher storeys had better ventilation potential.

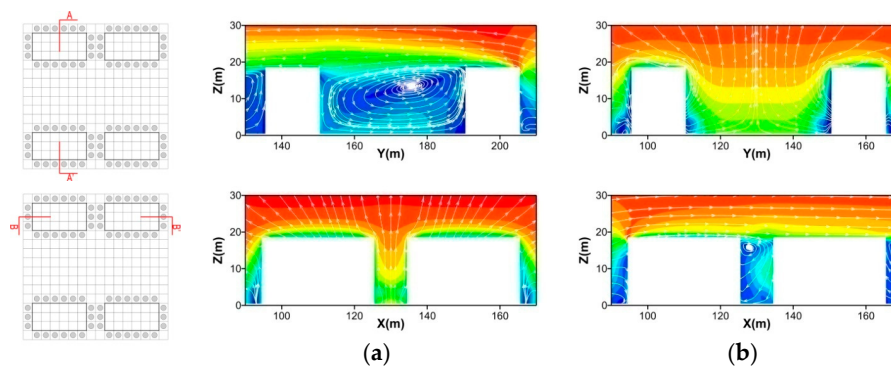


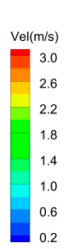
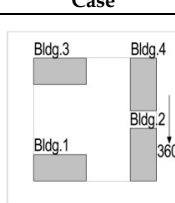
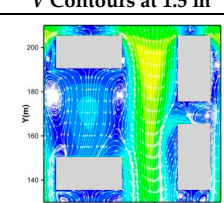
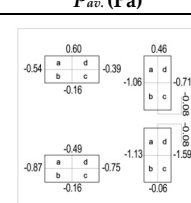
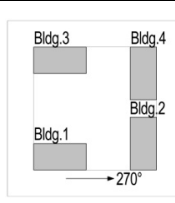
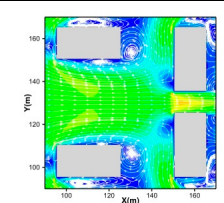
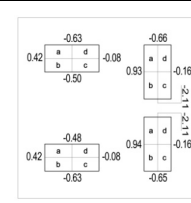
**Figure 4.** Velocity contours and streamlines presented at vertical sections of configuration 1 when the wind angle was 360° (a) and 270° (b), respectively.

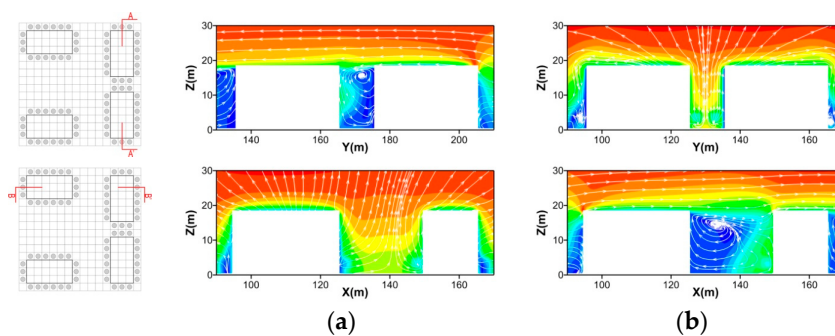
5.1.2. Configuration 2

Table 4 depicts contours of velocity and streamline distributions for  $Z = 1.5$  m, the average wind pressure on facades, and the wind pressure difference across flats in configuration 2. In the  $360^\circ$  wind direction scenario, the central space between Buildings 1 and 3, where airflow reversed significantly and exerted obvious vortices, was wind shaded. The left vortex was stronger than the right vortex. An analysis of the  $270^\circ$  wind direction indicated that airflow passes through the large area between windward buildings, and encountered leeward buildings, resulting in a partial separation. The wind converged between two gables of leeward buildings and reached its maximum velocity in the convergence area. There are more vortices revealed by comparing these, in the case of the  $360^\circ$  wind direction (Figure 5a,b).

By analyzing the results of different wind directions, it was found that the highest absolute values of wind pressure difference all occurred in Building 2. In the case of the  $360^\circ$  wind direction, wind pressure increased with height for Flats *b* and *c* of Building 1. For Building 2, Flats *a* and *d* experienced low wind pressure differences, with values of  $-0.34$  and  $-0.79$  Pa, respectively. Flats *b* and *c* in Building 3 had negative values, but positive values in Flats *a* and *d*. In the case of the  $270^\circ$  wind direction, it was only necessary to analyze Buildings 1 and 2. For Building 1, the absolute value of wind pressure differences ranged from  $-0.40$  to  $1.06$  Pa. Flats *a* and *b* had positive values of  $0.90$  and  $1.06$  Pa, respectively. Flat *a* had the highest values compared with other flats in Building 2. The total absolute wind pressure difference of Building 2 was higher than that of Building 1, with a difference of  $4.16$  Pa.

**Table 4.** Results of configuration 2 showing velocity contours and streamlines around blocks at 1.5 m height (m/s), average wind pressure on facades,  $P_{av.}$  (Pa), and pressure differences across each flat,  $dP$ , (Pa).

V	Case	V Contours at 1.5 m	$P_{av.}$ (Pa)	$dP$ across Flats <i>a</i> to <i>d</i> (Pa)				
				Block No.				
				Bldg.1	Bldg.2	Bldg.3	Bldg.4	
				a	-0.38	-0.34	1.14	1.52
				b	0.71	1.07	-0.38	-0.98
				c	0.59	1.52	-0.23	-0.63
				d	-0.26	-0.79	0.99	1.16
				a	0.90	3.05	1.05	1.59
				b	1.06	1.58	0.92	3.05
				c	-0.55	-0.49	-0.41	-1.95
				d	-0.40	-1.95	-0.55	-0.50



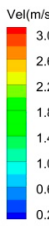
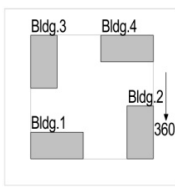
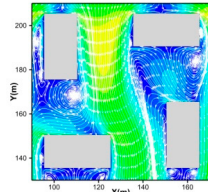
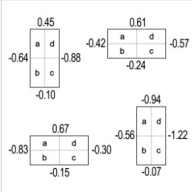
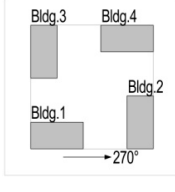
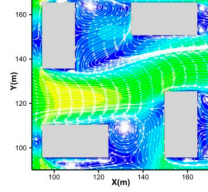
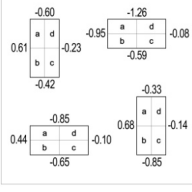
**Figure 5.** Velocity contours and streamlines presented at vertical sections of configuration 2 when the wind angle was  $360^\circ$  (a), and  $270^\circ$  (b), respectively.

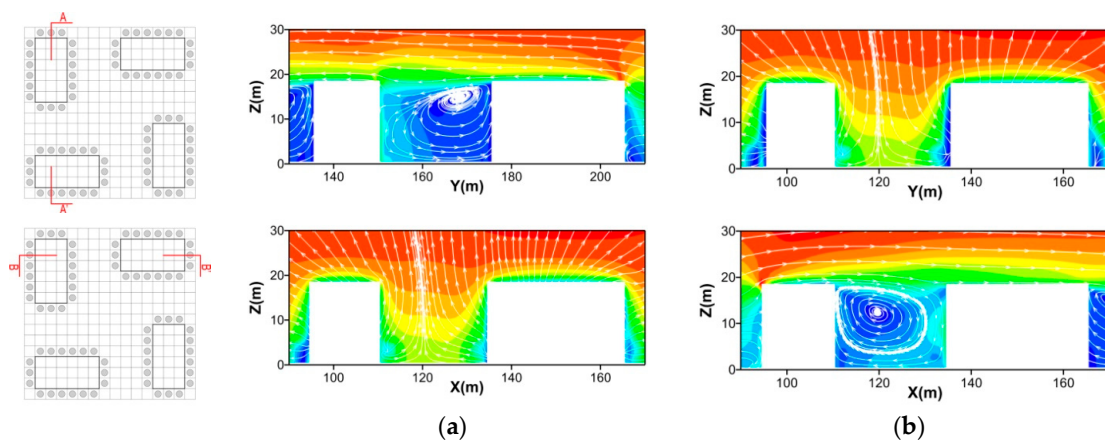
### 5.1.3. Configuration 3

Table 5 shows the contours of velocity and streamline distributions at the pedestrian level, the average wind pressure on facades, and the wind pressure difference across flats in configuration 3. The results of the leeward and windward aspects in the 360° wind direction were the same for those when the wind direction was 270°. Buildings 3, 4, 1, and 2 in the case of the 360° wind were equivalent to Buildings 1, 3, 2, and 4 at the 270° wind direction. Thus, it is only necessary to analyze the contours of velocities and  $dP$  across each flat for the 360° wind direction.

An analysis of streamline distributions indicated that airflow penetrated the central space between windward buildings and converged near the long facade of Building 2. The area between Buildings 4 and 2 with trees created wind deflection, resulting in obvious reversed flow and small vortexes (Figure 6a,b). The resulting wind pressure difference ranged from  $-0.68$  to  $1.51$  Pa of Building 1. The special tendency for Building 2 is that airflow travels from indoors to outdoors at the lower height and oppositely at the upper height. There is a sharp velocity increase in the top of Buildings 3 and 4, and the two blocks have the same tendency for having a higher absolute value of pressure difference, with values of  $3.71$  Pa and  $2.72$  Pa, respectively.

**Table 5.** Results of configuration 3 showing velocity contours and streamlines around blocks at 1.5 m height (m/s), average wind pressure on facades,  $P_{av.}$ , (Pa), and pressure differences across each flat,  $dP$ , (Pa).

V	Case	V Contours at 1.5 m	$P_{av.}$ (Pa)	$dP$ across Flats a to d (Pa)				
				Block No.				
				Bldg.1	Bldg.2	Bldg.3	Bldg.4	
				Block No.				
				Bldg.1	Bldg.2	Bldg.3	Bldg.4	
				a	1.51	-0.38	1.09	1.03
				b	-0.68	0.49	-0.54	-0.18
				Block No.				
				Bldg.1	Bldg.2	Bldg.3	Bldg.4	
				a	1.29	1.00	1.21	0.31
				b	1.09	1.53	1.03	-0.36
			c	-0.55	-0.71	-0.19	0.51	
			d	-0.75	-0.19	-0.37	1.18	



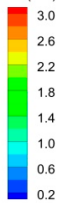
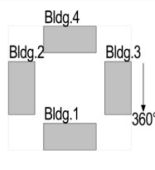
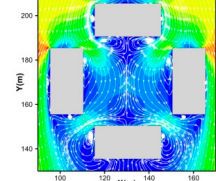
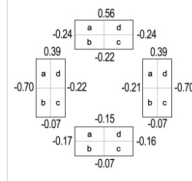
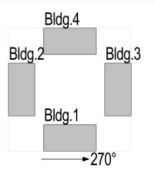
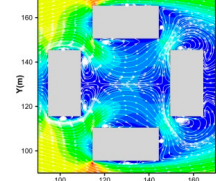
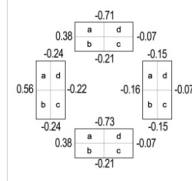
**Figure 6.** Velocity contours and streamlines presented at vertical sections of configuration 3 when the wind angle was 360° (a), and 270° (b), respectively.

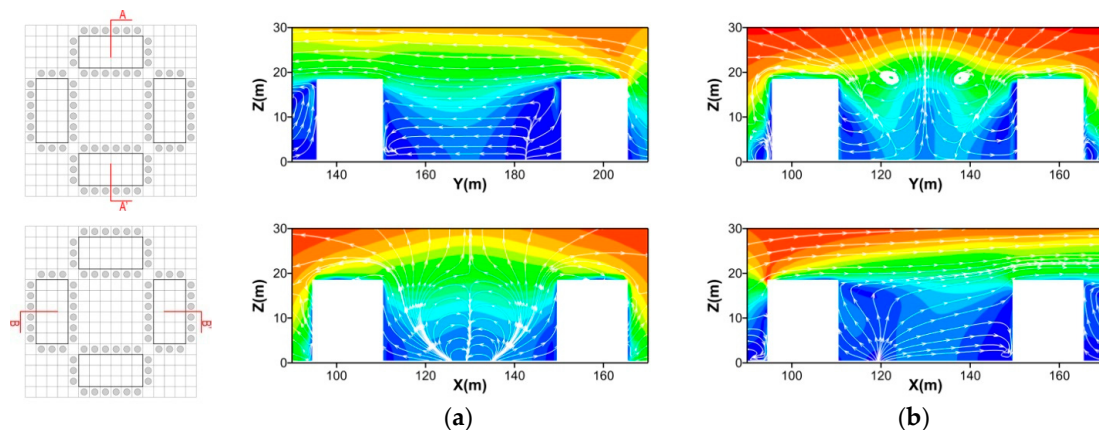
5.1.4. Configuration 4

Table 6 shows the results of the velocity contours around blocks and streamlines at  $Z = 1.5$  m (m/s), average wind pressure on facades, and pressure differences across each flat for configuration 4. The wind speed accelerated at the edge of Buildings 2 and 3 at the pedestrian level. Due to the narrow space for air to flow through, and the wind shading of the windward building, few airflows exerted slow movement in the central space created by the buildings envelope, and vortexes were small in each case (Figure 7a,b).

The absolute wind pressure differences were always near 0 Pa in the area surrounding Building 1, due to the wind-shading effect. Therefore, the flats in Building 1 had poor natural ventilation potential, and people may feel uncomfortable in interior space in this scenario. Flat *c* of Building 2 and Flat *b* of Building 3 both had slight improvements compared with other flats. In general, configuration 4 produced the poorest ventilation potential; as a result, it is the worst layout for airflow transportation.

**Table 6.** Results of configuration 4 showing velocity contours and streamlines around blocks at 1.5 m height (m/s), average wind pressure on facades,  $P_{av.}$  (Pa), and pressure differences across each flat,  $dP$ , (Pa).

V	Case	V Contours at 1.5 m	$P_{av.}$ (Pa)	$dP$ across Flats <i>a</i> to <i>d</i> (Pa)				
				Block No.				
				Bldg.1	Bldg.2	Bldg.3	Bldg.4	
				a	-0.02	1.09	0.60	0.81
				b	-0.09	-0.63	-0.14	-0.03
				c	-0.09	-0.15	-0.63	-0.02
				d	-0.01	0.61	1.09	0.81
				Block No.				
				Bldg.1	Bldg.2	Bldg.3	Bldg.4	
				a	0.59	0.80	0.01	1.09
				b	1.11	0.81	0.01	0.59
				c	-0.66	-0.03	-0.08	-0.14
				d	-0.14	-0.02	-0.08	-0.64



**Figure 7.** Velocity contours and streamlines presented at vertical sections of configuration 4 when the wind angle was  $360^\circ$  (a) and  $270^\circ$  (b), respectively.

5.2. Analysis of Indoor/Outdoor PM<sub>2.5</sub>

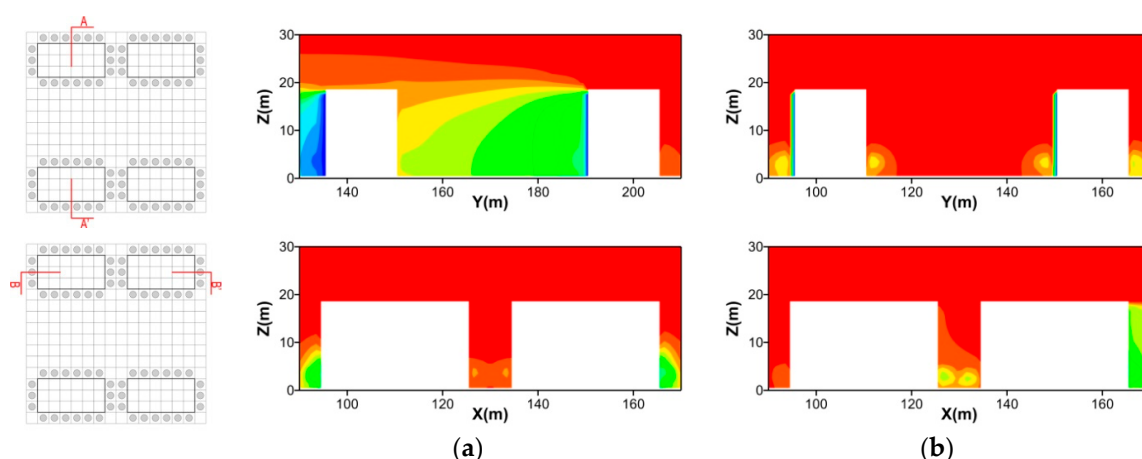
5.2.1. Configuration 1

Table 7 depicts the PM<sub>2.5</sub> concentrations around blocks at 1.5 m height, the average vertical PM<sub>2.5</sub> concentrations, and the indoor concentration across each flat for configuration 1. At a 360° wind direction, long building facades, except the windward facade of leeward buildings, remained the lowest PM<sub>2.5</sub> within tree crown height. The leeward facades of Buildings 1 and 2 had low particle concentrations on both lateral sides. On the leeward facades of buildings, particles were significantly affected by trees, and the deposition effect continued to the tops of buildings; however, its influence appeared only near the tree crown for windward building facades (Figure 8a). In the case of a 270° wind direction, the concentration distributions of lower layer for leeward facades of Buildings 1 and 3 were uniform. Thus, Buildings 1 and 2 need analysis. The leeward facades of Building 2 had lower concentrations when Z < 3 m, and the concentrations declined when 135 m < X < 140 m. The leeward facade of Building 1 had a lower concentration within the tree crown, and the deposition effects of trees on particulate matters reached to Z = 6 m (Figure 8b).

With a 360° wind direction, the PM<sub>2.5</sub> distributions around Buildings 1 and 3 were symmetrical to Buildings 2 and 4. Therefore, the indoor concentrations of Buildings 1 and 3 need to be analyzed. The concentrations of the leeward building (Building 1) were significantly lower than that of the windward building (Building 3), with a difference of 59.6 µg/m<sup>3</sup>. In Building 1, the PM<sub>2.5</sub> of Flats b and c were lower, with the values of 26.5 and 28.8 µg/m<sup>3</sup>, which meant 20% of the inlet value. The concentrations of Flats b and c in Building 3 were the lowest, and Flat d was the highest, with the value of 76.0 µg/m<sup>3</sup>. The results from a 270° wind direction showed that the concentrations of each flat were similar with a difference of 3.3 µg/m<sup>3</sup>, and Flats a and b in Building 1 had maximum concentrations, with 74.7 and 75.9 µg/m<sup>3</sup>, respectively. The concentrations for each flat of Building 2 ranked lowest to highest in order are: Flat c < Flat d < Flat b < Flat a.

**Table 7.** Results of configuration 1 showing PM<sub>2.5</sub> concentrations around blocks at 1.5 m height (µg/m<sup>3</sup>), average vertical PM<sub>2.5</sub> concentrations (0.5 m away from facades), (µg/m<sup>3</sup>), and indoor C<sub>av</sub> across flats a to d, (µg/m<sup>3</sup>).

C	Case	C Contours at 1.5 m	Outdoor Vertical C <sub>av</sub> (µg/m <sup>3</sup> )	Indoor C <sub>av</sub> across Flats a to d (µg/m <sup>3</sup> )																																			
				Block No.																																			
				Bldg.1	Bldg.2	Bldg.3	Bldg.4																																
			<table border="1"> <tr> <td>130.7</td> <td>130.5</td> <td>130.6</td> <td>130.7</td> </tr> <tr> <td>a</td> <td>d</td> <td>a</td> <td>d</td> </tr> <tr> <td>b</td> <td>c</td> <td>b</td> <td>c</td> </tr> <tr> <td>83.7</td> <td>83.9</td> <td>83.8</td> <td>83.7</td> </tr> </table> <table border="1"> <tr> <td>119.4</td> <td>115.9</td> <td>116.0</td> <td>119.3</td> </tr> <tr> <td>a</td> <td>d</td> <td>a</td> <td>d</td> </tr> <tr> <td>b</td> <td>c</td> <td>b</td> <td>c</td> </tr> <tr> <td>44.5</td> <td>44.5</td> <td>44.4</td> <td>44.0</td> </tr> </table>	130.7	130.5	130.6	130.7	a	d	a	d	b	c	b	c	83.7	83.9	83.8	83.7	119.4	115.9	116.0	119.3	a	d	a	d	b	c	b	c	44.5	44.5	44.4	44.0	Block No.			
				130.7	130.5	130.6	130.7																																
				a	d	a	d																																
				b	c	b	c																																
	83.7	83.9	83.8	83.7																																			
	119.4	115.9	116.0	119.3																																			
	a	d	a	d																																			
	b	c	b	c																																			
44.5	44.5	44.4	44.0																																				
a	64.7	64.8	68.4	76.0																																			
b	26.5	28.7	50.6	49.2																																			
c	28.8	26.2	49.4	50.9																																			
d	64.8	64.6	76.0	68.4																																			
		<table border="1"> <tr> <td>127.4</td> <td>126.2</td> <td>122.5</td> <td>124.2</td> </tr> <tr> <td>a</td> <td>d</td> <td>a</td> <td>d</td> </tr> <tr> <td>b</td> <td>c</td> <td>b</td> <td>c</td> </tr> <tr> <td>131.3</td> <td>118.7</td> <td>125.8</td> <td>126.0</td> </tr> </table> <table border="1"> <tr> <td>131.1</td> <td>117.3</td> <td>125.7</td> <td>125.8</td> </tr> <tr> <td>a</td> <td>d</td> <td>a</td> <td>d</td> </tr> <tr> <td>b</td> <td>c</td> <td>b</td> <td>c</td> </tr> <tr> <td>127.9</td> <td>127.1</td> <td>122.8</td> <td>124.6</td> </tr> </table>	127.4	126.2	122.5	124.2	a	d	a	d	b	c	b	c	131.3	118.7	125.8	126.0	131.1	117.3	125.7	125.8	a	d	a	d	b	c	b	c	127.9	127.1	122.8	124.6	Block No.				
			127.4	126.2	122.5	124.2																																	
			a	d	a	d																																	
			b	c	b	c																																	
131.3	118.7	125.8	126.0																																				
131.1	117.3	125.7	125.8																																				
a	d	a	d																																				
b	c	b	c																																				
127.9	127.1	122.8	124.6																																				
a	74.7	71.1	73.6	69.5																																			
b	75.9	69.4	74.8	70.9																																			
c	74.1	66.5	73.1	68.1																																			
d	72.6	68.1	75.3	66.4																																			



**Figure 8.** PM<sub>2.5</sub> concentrations presented at vertical sections of configuration 1 when the wind angle is 360° (a), and 270° (b), respectively.

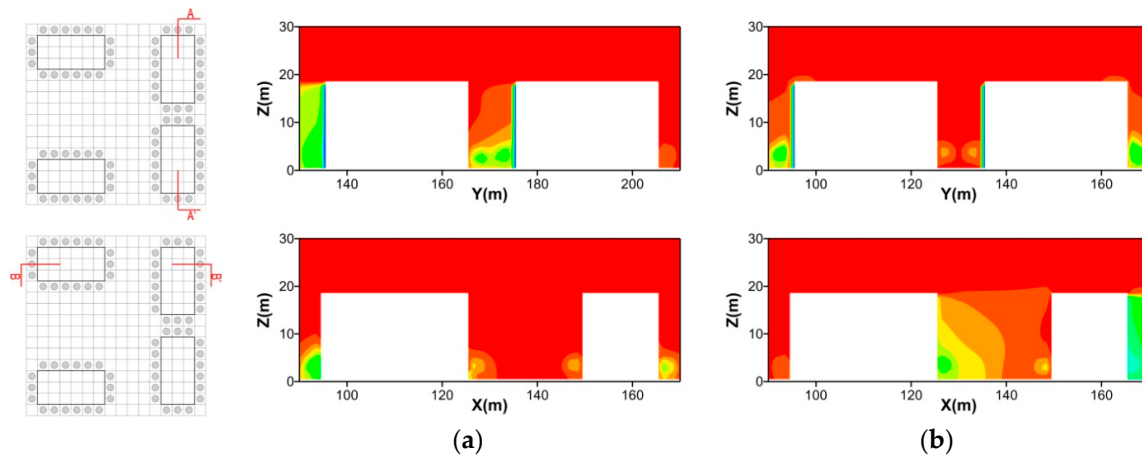
### 5.2.2. Configuration 2

Table 8 depicts PM<sub>2.5</sub> concentrations around blocks at 1.5 m height, the average vertical PM<sub>2.5</sub> concentrations, and the indoor concentration across each flat for configuration 2. In the case of a 360° wind direction, the concentrations of the leeward façade of Building 1 were lower than that of other façades, and showed significant decreases within the tree crown. The concentration distributions of the vertical façades of Building 3 were similar to those of Building 1. Meanwhile, the concentrations of windward and leeward façades of Building 2 were the lowest within the height of the tree crown. The indoor particle concentrations of Buildings 1 and 3 were lower than Buildings 2 and 4. Flats *b* and *c* had lower concentrations compared with Flats *a* and *d* for Building 1, and the lowest concentrations appeared at the height within tree crown height (from 2 m to 5 m). For Building 2, the PM<sub>2.5</sub> had no obvious change, and the indoor average values ranged from 64.3 to 69.8 µg/m<sup>3</sup>. In Building 3, the concentrations of Flats *b* and *c* varied in the same way, and the influence of the surrounding trees continued to the top of the buildings. In Building 4, the concentrations of Flats *b* and *c* were similar from the bottom to the top of the building (Figure 9a).

**Table 8.** Results of configuration 2 showing PM<sub>2.5</sub> concentrations around blocks at 1.5 m height (µg/m<sup>3</sup>), average vertical PM<sub>2.5</sub> concentrations (0.5 m away from façades), (µg/m<sup>3</sup>), and indoor C<sub>av</sub> across flats *a* to *d*, (µg/m<sup>3</sup>).

C	Case	C Contours at 1.5 m	Outdoor Vertical C <sub>av</sub> (µg/m <sup>3</sup> )	Indoor C <sub>av</sub> across Flats <i>a</i> to <i>d</i> (µg/m <sup>3</sup> )																																																													
			<table border="1"> <tr><td>131.2</td><td>131.2</td></tr> <tr><td>a</td><td>d</td></tr> <tr><td>b</td><td>c</td></tr> <tr><td>84.1</td><td>84.1</td></tr> </table> <table border="1"> <tr><td>131.4</td><td>a</td><td>d</td><td>126.6</td></tr> <tr><td>128.0</td><td>b</td><td>c</td><td>128.5</td></tr> </table> <table border="1"> <tr><td>119.5</td><td>119.3</td></tr> <tr><td>a</td><td>d</td></tr> <tr><td>b</td><td>c</td></tr> <tr><td>73.9</td><td>76.5</td></tr> </table> <table border="1"> <tr><td>125.2</td><td>a</td><td>d</td><td>124.3</td></tr> <tr><td>124.1</td><td>b</td><td>c</td><td>125.0</td></tr> </table>	131.2	131.2	a	d	b	c	84.1	84.1	131.4	a	d	126.6	128.0	b	c	128.5	119.5	119.3	a	d	b	c	73.9	76.5	125.2	a	d	124.3	124.1	b	c	125.0	<table border="1"> <tr><th colspan="4">Block No.</th></tr> <tr><th></th><th>Bldg.1</th><th>Bldg.2</th><th>Bldg.3</th><th>Bldg.4</th></tr> <tr><th>a</th><td>69.6</td><td>69.8</td><td>74.6</td><td>68.2</td></tr> <tr><th>b</th><td>46.7</td><td>66.0</td><td>54.2</td><td>69.6</td></tr> <tr><th>c</th><td>49.6</td><td>64.3</td><td>53.7</td><td>74.3</td></tr> <tr><th>d</th><td>69.8</td><td>66.8</td><td>76.9</td><td>72.1</td></tr> </table>	Block No.					Bldg.1	Bldg.2	Bldg.3	Bldg.4	a	69.6	69.8	74.6	68.2	b	46.7	66.0	54.2	69.6	c	49.6	64.3	53.7	74.3	d	69.8	66.8	76.9	72.1
	131.2	131.2																																																															
a	d																																																																
b	c																																																																
84.1	84.1																																																																
131.4	a	d	126.6																																																														
128.0	b	c	128.5																																																														
119.5	119.3																																																																
a	d																																																																
b	c																																																																
73.9	76.5																																																																
125.2	a	d	124.3																																																														
124.1	b	c	125.0																																																														
Block No.																																																																	
	Bldg.1	Bldg.2	Bldg.3	Bldg.4																																																													
a	69.6	69.8	74.6	68.2																																																													
b	46.7	66.0	54.2	69.6																																																													
c	49.6	64.3	53.7	74.3																																																													
d	69.8	66.8	76.9	72.1																																																													
		<table border="1"> <tr><td>127.0</td><td>125.6</td></tr> <tr><td>a</td><td>d</td></tr> <tr><td>b</td><td>c</td></tr> <tr><td>131.1</td><td>118.0</td></tr> </table> <table border="1"> <tr><td>129.6</td><td>a</td><td>d</td><td>82.7</td></tr> <tr><td>130.8</td><td>b</td><td>c</td><td>86.4</td></tr> </table> <table border="1"> <tr><td>131.0</td><td>116.7</td></tr> <tr><td>a</td><td>d</td></tr> <tr><td>b</td><td>c</td></tr> <tr><td>127.4</td><td>126.3</td></tr> </table> <table border="1"> <tr><td>130.9</td><td>a</td><td>d</td><td>85.7</td></tr> <tr><td>129.6</td><td>b</td><td>c</td><td>81.9</td></tr> </table>	127.0	125.6	a	d	b	c	131.1	118.0	129.6	a	d	82.7	130.8	b	c	86.4	131.0	116.7	a	d	b	c	127.4	126.3	130.9	a	d	85.7	129.6	b	c	81.9	<table border="1"> <tr><th colspan="4">Block No.</th></tr> <tr><th></th><th>Bldg.1</th><th>Bldg.2</th><th>Bldg.3</th><th>Bldg.4</th></tr> <tr><th>a</th><td>71.8</td><td>77.1</td><td>70.1</td><td>65.5</td></tr> <tr><th>b</th><td>73.0</td><td>65.5</td><td>71.9</td><td>77.1</td></tr> <tr><th>c</th><td>70.4</td><td>50.9</td><td>70.3</td><td>55.4</td></tr> <tr><th>d</th><td>70.1</td><td>55.1</td><td>72.6</td><td>51.5</td></tr> </table>	Block No.					Bldg.1	Bldg.2	Bldg.3	Bldg.4	a	71.8	77.1	70.1	65.5	b	73.0	65.5	71.9	77.1	c	70.4	50.9	70.3	55.4	d	70.1	55.1	72.6	51.5	
127.0	125.6																																																																
a	d																																																																
b	c																																																																
131.1	118.0																																																																
129.6	a	d	82.7																																																														
130.8	b	c	86.4																																																														
131.0	116.7																																																																
a	d																																																																
b	c																																																																
127.4	126.3																																																																
130.9	a	d	85.7																																																														
129.6	b	c	81.9																																																														
Block No.																																																																	
	Bldg.1	Bldg.2	Bldg.3	Bldg.4																																																													
a	71.8	77.1	70.1	65.5																																																													
b	73.0	65.5	71.9	77.1																																																													
c	70.4	50.9	70.3	55.4																																																													
d	70.1	55.1	72.6	51.5																																																													

With a  $270^\circ$  wind direction, the patterns of Buildings 1 and 3 were symmetrical to Buildings 2 and 4. So, the results of Buildings 1 and 2 must be analyzed. The concentrations appeared lower on the leeward facades of back buildings, and decreased within the tree canopy. For Building 1, concentrations of Flat *a* gradually decreased with the building height. Flats *c* and *d* had lower concentrations, with a value of approximately  $70 \mu\text{g}/\text{m}^3$ . The concentrations for the flats of Building 2, ranked lowest to highest, in order, are: Flat *c* < Flat *d* < Flat *b* < Flat *a*. Flats *c* and *d* have the lowest concentrations, with the values of  $50.9$  and  $55.1 \mu\text{g}/\text{m}^3$ , respectively (Figure 9b).



**Figure 9.**  $\text{PM}_{2.5}$  concentrations presented at vertical sections of configuration 2 when the wind angle was  $360^\circ$  (a) and  $270^\circ$  (b), respectively.

### 5.2.3. Configuration 3

Table 9 depicts  $\text{PM}_{2.5}$  concentrations around blocks at 1.5 m height, the average vertical  $\text{PM}_{2.5}$  concentrations, and the indoor concentration across each flat for configuration 3. The building layout in configuration 3 is centrally symmetrical; hence, only the indoor and outdoor particle concentrations distribution at  $360^\circ$  wind needs to be analyzed. The concentrations of the leeward facade of Building 1 were significantly lower than the other facades, and reached their lowest values within the tree canopy. The low concentrations of the long facades of Buildings 3 and 4 also occurred within the tree canopy, while the concentrations of the long facades of Building 2 increased with the building height (Figure 10). An analysis of indoor  $\text{PM}_{2.5}$  concentrations showed that the concentrations of Flats *b* and *c* were low in Building 1, with the values of  $45.1 \mu\text{g}/\text{m}^3$  and  $48.3 \mu\text{g}/\text{m}^3$ , respectively. In Building 2, the concentrations of Flats *b* and *c* differed indistinctly. In Building 3, the concentrations of Flat *b* changed obviously between each storey, with the maximum concentration occurring at the 5 m height. The concentrations of Flats *b* and *c* represented lower values in Building 4, with values of  $64.8 \mu\text{g}/\text{m}^3$  and  $64.9 \mu\text{g}/\text{m}^3$ .

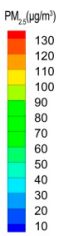
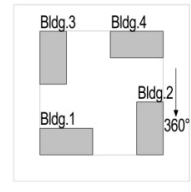
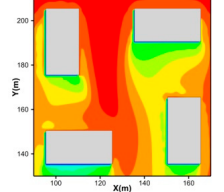
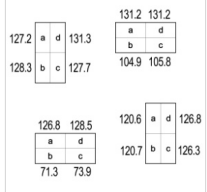
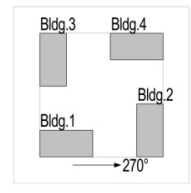
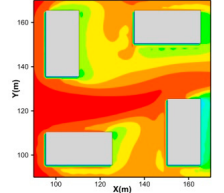
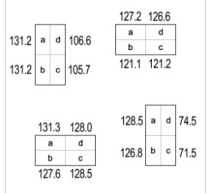
### 5.2.4. Configuration 4

Table 10 shows  $\text{PM}_{2.5}$  concentrations around blocks at 1.5 m height, the average vertical concentration, and the indoor concentrations across Flats *a* to *d* in configuration 4. This layout is also centrally symmetrical. In the scenario with an angle of  $360^\circ$ , the concentrations of leeward facade of Building 1 were lower within the tree crown, and the deposition effects reached to 15 m on both lateral sides of the building facades. These deposition effects on the windward facade of Building 2 reached to 12 m (the fourth storey). The concentrations of the leeward facade of Building 2 also obtained their minimum values within the tree canopy. Buildings 2 and 3 were symmetrical for all four flats. The concentrations of the leeward facade of Building 4 gradually increased from the middle to the top of the building (Figure 11). An analysis of indoor  $\text{PM}_{2.5}$  indicated that Flats *b* and *c* have the



same change tendency, with a lower value of  $24.7 \mu\text{g}/\text{m}^3$  and  $24.6 \mu\text{g}/\text{m}^3$ , respectively. In Building 2, the concentrations of Flat *d* reached the lowest value compared with other flats. Building 3 was symmetrical with Building 2, and their changes were similar. In Building 4, the concentrations of Flats *b* and *c* were similar. Flats *a* and *d* have the same changes that occur elsewhere along the vertical facades.

**Table 9.** Results of configuration 3 showing  $\text{PM}_{2.5}$  concentrations around blocks at 1.5 m height ( $\mu\text{g}/\text{m}^3$ ), average vertical  $\text{PM}_{2.5}$  concentrations (0.5 m away from facades), ( $\mu\text{g}/\text{m}^3$ ), and indoor  $C_{av}$  across flats *a* to *d*, ( $\mu\text{g}/\text{m}^3$ ).

C	Case	C Contours at 1.5 m	Outdoor Vertical $C_{av}$ ( $\mu\text{g}/\text{m}^3$ )	Indoor $C_{av}$ across Flats <i>a</i> to <i>d</i> ( $\mu\text{g}/\text{m}^3$ )				
				Block No.				
				Block No.				
					<i>Bldg.1</i>	<i>Bldg.2</i>	<i>Bldg.3</i>	<i>Bldg.4</i>
				<i>a</i>	68.9	74.4	71.7	77.0
				<i>b</i>	45.1	67.0	74.5	64.8
					Block No.			
					<i>Bldg.1</i>	<i>Bldg.2</i>	<i>Bldg.3</i>	<i>Bldg.4</i>
	<i>a</i>				68.5	75.1	73.8	69.0
	<i>b</i>				71.9	69.0	77.0	74.3
<i>c</i>	74.7	45.3	65.5	66.8				
<i>d</i>	71.8	49.1	65.4	65.7				

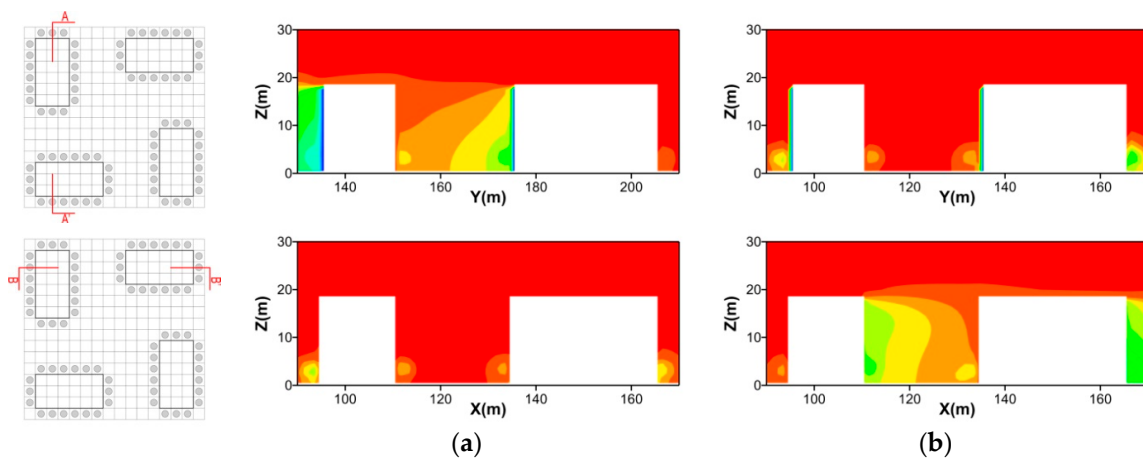


**Figure 10.**  $\text{PM}_{2.5}$  concentrations presented at vertical sections of configuration 3 when the wind angle was  $360^\circ$  (a), and  $270^\circ$  (b), respectively.

The above-mentioned discussion aimed at exploring the resulting ventilation potential and outdoor and indoor  $\text{PM}_{2.5}$  concentrations of each configuration. However, the question of which configuration can give the best ventilation potential, which can provide the lowest indoor  $\text{PM}_{2.5}$  concentrations, and the relationship between wind pressure difference and indoor  $\text{PM}_{2.5}$  concentrations remain outstanding. Thus, further assessments of each scenario considering the actual architectural and tree planting design were conducted. A general assessment can be given by summing up the pressure difference values and indoor  $\text{PM}_{2.5}$  across the sixteen flats of each configuration. Since positive or negative pressure differences only indicate the flow direction, pressure differences should be converted to their absolute values when summed.

**Table 10.** Results of configuration 4 showing PM<sub>2.5</sub> concentrations around blocks at 1.5 m height (μg/m<sup>3</sup>), average vertical PM<sub>2.5</sub> concentrations (0.5 m away from facades), (μg/m<sup>3</sup>), and indoor C<sub>av</sub> across flats a to d, (μg/m<sup>3</sup>).

C	Case	C Contours at 1.5 m	Outdoor Vertical C <sub>av</sub> (μg/m <sup>3</sup> )	Indoor C <sub>av</sub> across Flats a to d (μg/m <sup>3</sup> )				
				Bldg.1	Bldg.2	Bldg.3	Bldg.4	
	360°			Block No.				
				a	73.6	68.1	61.1	71.4
				b	24.7	69.4	75.8	64.4
	c	24.6	75.6	69.3	64.2			
	d	73.6	60.7	67.8	71.4			
	270°			Block No.				
a				61.2	71.4	73.3	67.7	
b				68.0	71.4	73.3	61.5	
c	69.1	64.1	27.6	75.9				
d	75.9	63.7	27.6	69.1				

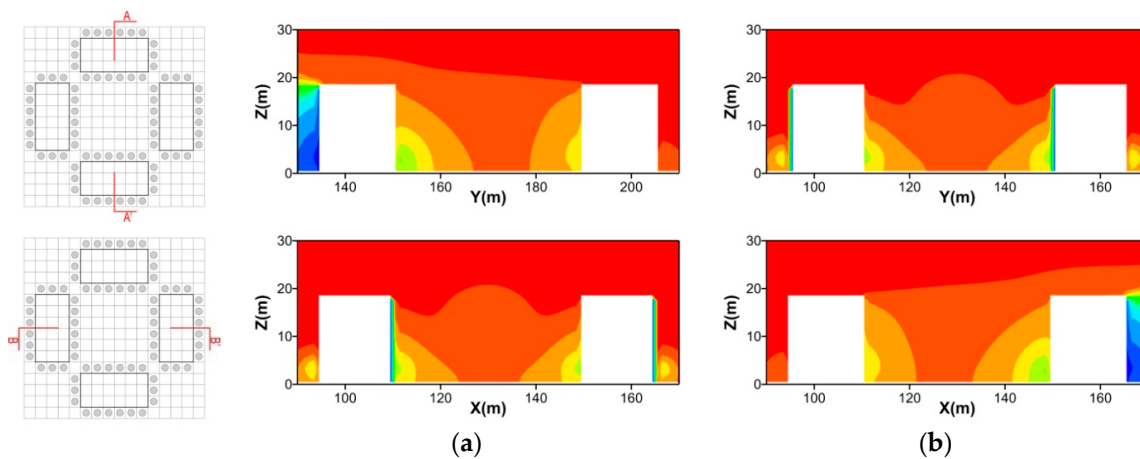


**Figure 11.** PM<sub>2.5</sub> concentrations presented at a vertical section of configuration 4 when the wind angle was 360° (a) and 270° (b), respectively.

Figure 12 depicts the total absolute values for pressure differences and interior PM<sub>2.5</sub> concentrations with the wind directions of 360° and 270°. The high pressure difference in configuration 2 with a 270° wind direction results in the best ventilation potential. The poorest ventilation potential is found in configuration 4, in two wind directions with similar wind pressure differences because of the wind-shading effect. This scenario showed 7.51 Pa and 2.70 Pa, respectively, which means a difference of 178% (Figure 12a). Configuration 1 had the lowest indoor PM<sub>2.5</sub> with the wind angle of 360°, and highest concentration with a 270° wind direction (Figure 12b). The overall values were similar among the other three configurations at different wind angles. A scatter plot of indoor PM<sub>2.5</sub> concentration versus wind pressure difference had an R<sup>2</sup> of 0.059 for PM<sub>2.5</sub> (Figure 12c).

The results of this study suggest that wind pressure difference has little effect on indoor PM<sub>2.5</sub> concentration. This is similar to the results concluded by Chithra and Shiva Nagendra [30]. It differs, however, from the simulation study using a CONTAMW simulation, as our study shows the lower floors of a multi-storey building having lower PM<sub>2.5</sub> compared with the upper floors. The CONTAMW simulation drew the opposite conclusion [68]. However, this was only because our study considered

the aerodynamic and deposition effects of trees on particles dispersion, and airflow fields among building complexes is different from single office buildings.

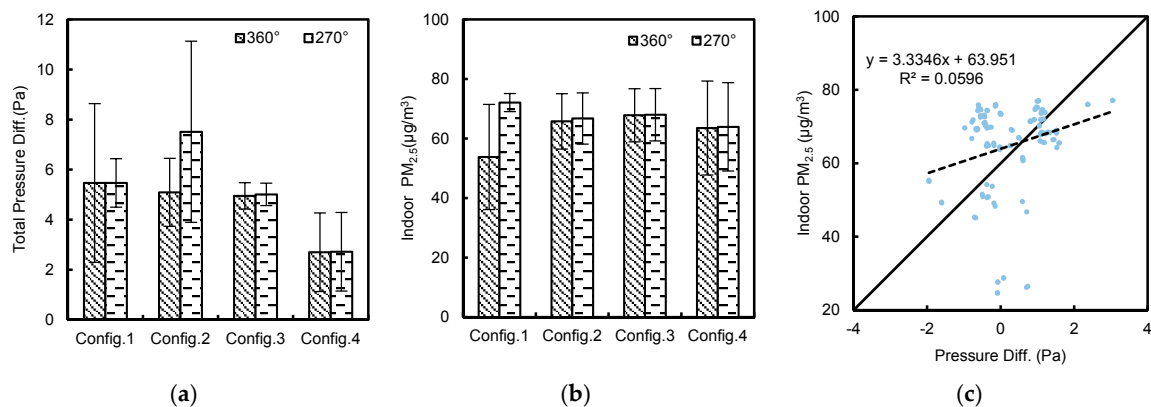


**Figure 12.** The resulting gross absolute pressure difference for each configuration (a), indoor PM<sub>2.5</sub> for each configuration (b), and correlation between indoor PM<sub>2.5</sub> and wind pressure difference (c). Dashed lines are linear fits, with linear equations and  $R^2$ -values given alongside. Diagonals depict perfect matches.

Our study found that lower floors are subject to less PM<sub>2.5</sub> than upper floors, because we assume that the pollution source was introduced through the inlet from a representative, dispersed upstream source. Based on regional statistics [45], the predominant source of PM<sub>2.5</sub> pollution in Beijing in 2015 was derived from atmospheric transmission, which accounted for 38.6% of all sources (e.g., traffic, industry, and burning). Thus, this study added the pollution source through the inlet. However, in many urban environments, the pollution source is at street level in the vicinity of the buildings. An indepth study should be carried out to consider this alternative scenario.

This research qualitatively and quantitatively assessed the airflow field and indoor/outdoor relationships for PM<sub>2.5</sub> within partly wind-driven natural ventilation in four typical building–tree configurations. Our study had some limitations that should be addressed. First, the airflow and particle dispersion simulation was only conducted for some building–tree patterns, and trees around the buildings were simulated as evergreen trees and planted aligned to the road. Additionally, weather parameters that were only typical during November to December in 2015 were used in this simulation study. Thus, more building and tree arrangements in serious climate conditions should be considered. Second, field experiments measuring the pressure difference and particle transportation indoor and outdoor in multi-storey buildings are needed in subsequent study to verify our conclusions. Third, particles are regarded as a continuum, and particle movements are assumed to not affect turbulence. The convective velocity of the particle phase is assumed to be the same as the airflow in this study. However, wind flow in the real environments is transient, and even a steady wind condition gives transient vortex shedding in wind-tunnel/field experiments under certain configurations [69]. These transient flows are important, both for pollutant mixing and building ventilation. Thus, an experimental validation of the models is still needed. Fourth, the findings of this study are only valid for wind-driven ventilation. There may be other mechanisms that are important under thermally-driven conditions, i.e., solar heat, anthropogenic heat, heat absorption/emission of building masses, etc. More complicated scenarios, such as non-isothermal cases with solar radiation, and convective heat transfer inside buildings and tree clusters, would add to our findings. Finally, this study assumed that the pollution sources were diluted by wind transportation, and the indoor generation of particles was not considered. This is because the objective of this research was to explore the effects of building–tree patterns on indoor particle concentrations generated outdoors. In the real built environment, indoor air pollution is affected not only by outdoor pollution,

but also by indoor originated particles. A comprehensive analysis linking various factors of I/O ratio, particle penetration, and infiltration, and indoor generated could contribute to a thorough understanding of actual indoor/outdoor particles dispersion in multi-storey buildings with different building–tree arrangements.

## 6. Conclusions

In this study, the effects of four typical building–tree configurations on the pedestrian-level wind environment, the wind pressure on building facades, and the indoor/outdoor relationships for PM<sub>2.5</sub> due to partly wind-driven natural ventilation were studied by the standard  $k$ - $\epsilon$  model and the revised generalized drift flux model. The results clearly indicated that airflow and indoor/outdoor PM<sub>2.5</sub> dispersion strongly depended on the relationships of building layouts, tree arrangements, and orientation towards the prevailing wind. The following conclusions can be drawn from the simulated results: (1) Building and tree configurations can provide natural ventilation potentials relying on wind influence, and buildings that experience wind deflection on their windward facade and airflow separation on the leeward side have better ventilation potential; (2) Patterns with buildings and trees forming a central space and an opening side towards the prevailing wind could offer the best ventilation conditions, that is to say, configuration 2 with the prevailing wind direction of 270° can offer the best ventilation potential, and a great difference of 178% existed when comparing it with the poorest configuration; (3) Under the conditions of the particle sources introduced to the interior through the inlet, the aerodynamics and deposition effects of trees allowed the lower floors of a multi-storey building to be exposed to lower PM<sub>2.5</sub> compared with the upper storeys. As well, lower indoor PM<sub>2.5</sub> were found close to the tree canopy, leading to a significant reduction on PM<sub>2.5</sub> with the height of tree canopy; (4) Wind pressure differences across each flat showed poor correlation ( $R^2 = 0.059$ ) with indoor PM<sub>2.5</sub>. This is because pressure change usually causes global pollutant dispersion changes, rather than producing effects on microscopic pollutants dispersion [70]; and (5) Configurations with long building facades and trees perpendicular to prevailing wind had the lowest indoor PM<sub>2.5</sub>. The highest PM<sub>2.5</sub> was observed in configuration 1 with a 270° wind direction, while the lowest was also observed in configuration 1, with a wind angle of 360°. This emphasized the importance of prevailing wind in the transportation of pollution.

**Acknowledgments:** This study is supported by the National Natural Science Foundation of China (51708451, 51561135001 and 51638003) and the Innovative Research Groups of the National Natural Science Foundation of China (51521005).

**Author Contributions:** Bo Hong and Borong Lin conceived and designed the experiments; Bo Hong and Hongqiao Qin performed the experiments and analyzed the data; Bo Hong wrote the paper.

**Conflicts of Interest:** The authors declare no conflict of interest.

## References

1. Brunekreef, B.; Holgate, S.T. Air pollution and health. *Lancet* **2002**, *360*, 1233–1242. [[CrossRef](#)]
2. Zhang, X.; Zhang, X.; Chen, X. Happiness in the air: How does a dirty sky affect mental health and subjective well-being? *J. Environ. Econ. Manag.* **2017**, *85*, 81–94. [[CrossRef](#)] [[PubMed](#)]
3. Abt, E.; Suh, H.H.; Catalano, P.; Koutrakis, P. Relative contribution of outdoor and indoor particle sources to indoor concentrations. *Environ. Sci. Technol.* **2000**, *34*, 3579–3587. [[CrossRef](#)]
4. Ramachandran, G.; Adgate, J.L.; Pratt, G.C.; Sexton, K. Characterizing indoor and outdoor 15 minute average PM<sub>2.5</sub> concentrations in urban neighborhoods. *Aerosol Sci. Technol.* **2003**, *37*, 33–45. [[CrossRef](#)]
5. Schneider, T.; Jensen, K.A.; Clausen, P.A.; Afshari, A.; Gunnarsen, L.; Wählén, P.; Glasius, M.; Palmgren, F.; Nielsen, O.J.; Fogh, C.L. Prediction of indoor concentration of 0.5–4  $\mu\text{m}$  particles of outdoor origin in an uninhabited apartment. *Atmos. Environ.* **2004**, *38*, 6349–6359. [[CrossRef](#)]
6. Matson, U. Indoor and outdoor concentrations of ultrafine particles in some Scandinavian rural and urban areas. *Sci. Total Environ.* **2005**, *343*, 169–176. [[CrossRef](#)] [[PubMed](#)]
7. Jones, A.P. Indoor air quality and health. *Atmos. Environ.* **1999**, *33*, 4535–4564. [[CrossRef](#)]

8. Liao, C.M.; Huang, S.J.; Yu, H. Size-dependent particulate matter indoor/outdoor relationships for a wind-induced naturally ventilated airspace. *Build. Environ.* **2004**, *39*, 411–420. [[CrossRef](#)]
9. De Jong, T.; Bot, G.P.A. Air exchange caused by wind effects through (window) openings distributed evenly on a quasi-infinite surface. *Energy Build.* **1992**, *19*, 93–103. [[CrossRef](#)]
10. Miguel, A.F.; Van de Braak, N.J.; Silva, A.M.; Bot, G.P.A. Wind-induced airflow through permeable materials part I: Air infiltration in enclosure. *J. Wind Eng. Ind. Aerodyn.* **2001**, *89*, 59–72. [[CrossRef](#)]
11. Tominaga, Y.; Mochida, A.; Shirasawa, T.; Yoshie, R.; Kataoka, H.; Harimoto, K.; Nozu, T. Cross comparisons of CFD results of wind environment at pedestrian level around a high-rise building and with a building complex. *J. Asian Archit. Build.* **2004**, *3*, 63–70. [[CrossRef](#)]
12. Zhang, A.; Gao, C.; Zhang, L. Numerical simulation of the wind field around different building arrangements. *J. Wind Eng. Ind. Aerodyn.* **2005**, *93*, 891–904. [[CrossRef](#)]
13. Asfour, O.S.; Gadi, M.B. A comparison between CFD and Network models for predicting wind-driven ventilation in buildings. *Build. Environ.* **2007**, *42*, 4079–4085. [[CrossRef](#)]
14. Tominaga, Y.; Mochida, A.; Yoshie, R.; Kataoka, H.; Nozu, T.; Yoshikawa, M.; Shirasawa, T. AIJ guidelines for practical applications of CFD to pedestrian wind environment around buildings. *J. Wind Eng. Ind. Aerodyn.* **2008**, *96*, 1749–1761. [[CrossRef](#)]
15. Kubota, T.; Miura, M.; Tominaga, Y.; Mochida, A. Wind tunnel tests on the relationship between building density and pedestrian-level wind velocity: Development of guidelines for realizing acceptable wind environment in residential neighborhoods. *Build. Environ.* **2008**, *43*, 1699–1708. [[CrossRef](#)]
16. Mochida, A.; Lun, I.Y.F. Prediction of wind environment and thermal comfort at pedestrian level in urban area. *J. Wind Eng. Ind. Aerodyn.* **2008**, *96*, 1498–1527. [[CrossRef](#)]
17. Asfour, O.S. Prediction of wind environment in different grouping patterns of housing blocks. *Energy Build.* **2010**, *42*, 2061–2069. [[CrossRef](#)]
18. You, W.; Gao, Z.; Chen, Z.; Ding, W. Improving residential wind environments by understanding the relationship between building arrangements and outdoor regional ventilation. *Atmosphere* **2017**, *8*, 102. [[CrossRef](#)]
19. Mochida, A.; Tabata, Y.; Iwata, T.; Yoshino, H. Examining tree canopy models for CFD prediction of wind environment at pedestrian level. *J. Wind Eng. Ind. Aerodyn.* **2008**, *96*, 1667–1677. [[CrossRef](#)]
20. Chen, H.; Ooka, R.; Kato, S. Study on optimum design method for pleasant outdoor thermal environment using genetic algorithms (GA) and coupled simulation of convection, radiation and conduction. *Build. Environ.* **2008**, *43*, 18–30. [[CrossRef](#)]
21. Hong, B.; Lin, B.; Hu, L.; Li, S. Optimal tree design for sunshine and ventilation in residential district using geometrical models and numerical simulation. *Build. Simul.* **2011**, *4*, 351–363. [[CrossRef](#)]
22. Hong, B.; Lin, B.; Wang, B.; Li, S. Optimal design of vegetation in residential district with numerical simulation and field experiment. *J. Cent. South Univ.* **2012**, *19*, 688–695. [[CrossRef](#)]
23. Hong, B.; Lin, B. Numerical studies of the outdoor wind environment and thermal comfort at pedestrian level in housing blocks with different building layout patterns and trees arrangement. *Renew. Energy* **2015**, *73*, 18–27. [[CrossRef](#)]
24. Chen, C.; Zhao, B. Review of relationship between indoor and outdoor particles: I/O ratio, infiltration factor and penetration factor. *Atmos. Environ.* **2011**, *45*, 275–288. [[CrossRef](#)]
25. Braniš, M.; Řezáčová, P.; Domasová, M. The effect of outdoor air and indoor human activity on mass concentrations of PM<sub>10</sub>, PM<sub>2.5</sub>, and PM<sub>1</sub> in a classroom. *Environ. Res.* **2005**, *99*, 143–149. [[CrossRef](#)] [[PubMed](#)]
26. Massey, D.; Masih, J.; Kulshrestha, A.; Habil, M.; Taneja, A. Indoor/outdoor relationship of fine particles less than 2.5 μm (PM<sub>2.5</sub>) in residential homes locations in central Indian region. *Build. Environ.* **2009**, *44*, 2037–2045. [[CrossRef](#)]
27. Chithra, V.S.; Nagendra, S.M.S. Indoor air quality investigations in a naturally ventilated school building located close to an urban roadway in Chennai, India. *Build. Environ.* **2012**, *54*, 159–167. [[CrossRef](#)]
28. Mohammadyan, M.; Ghoochani, M.; Kloog, I.; Abdul-Wahab, S.A.; Yetilmezsoy, K.; Heibati, B.; Pollitt, K.J.G. Assessment of indoor and outdoor particulate air pollution at an urban background site in Iran. *Environ. Monit. Assess.* **2017**, *189*, 235. [[CrossRef](#)] [[PubMed](#)]

29. Hahn, I.; Brixy, L.A.; Wiener, R.W.; Henkle, S.W. Parameterization of meteorological variables in the process of infiltration of outdoor ultrafine particles into a residential building. *J. Environ. Monit.* **2009**, *11*, 2192–2200. [[CrossRef](#)] [[PubMed](#)]
30. Chithra, V.S.; Nagendra, S.M.S. Impact of outdoor meteorology on indoor PM<sub>10</sub>, PM<sub>2.5</sub> and PM<sub>1</sub> concentrations in a naturally ventilated classroom. *Urban Clim.* **2014**, *10*, 77–91. [[CrossRef](#)]
31. Riain, C.M.N.; Mark, D.; Davies, M.; Harrison, R.M.; Byrne, M.A. Averaging periods for indoor-outdoor ratios of pollution in naturally ventilated non-domestic buildings near a busy road. *Atmos. Environ.* **2003**, *37*, 4121–4132. [[CrossRef](#)]
32. Massey, D.; Kulshrestha, A.; Masih, J.; Taneja, A. Seasonal trends of PM<sub>10</sub>, PM<sub>5.0</sub>, PM<sub>2.5</sub> & PM<sub>1.0</sub> in indoor and outdoor environments of residential homes located in North-Central India. *Build. Environ.* **2012**, *47*, 223–231.
33. Zhao, X.; Zhang, X.; Xu, X.; Xu, J.; Meng, W.; Pu, W. Seasonal and diurnal variations of ambient PM<sub>2.5</sub> concentration in urban and rural environments in Beijing. *Atmos. Environ.* **2009**, *43*, 2893–2900. [[CrossRef](#)]
34. Yang, F.; Kang, Y.; Gao, Y.; Zhong, K. Numerical simulations of the effect of outdoor pollutants on indoor air quality of buildings next to a street canyon. *Build. Environ.* **2015**, *87*, 10–22. [[CrossRef](#)]
35. Zhao, B.; Zhang, Y.; Li, X.; Yang, X.; Huang, D. Comparison of indoor aerosol particle concentration and deposition in different ventilated rooms by numerical method. *Build. Environ.* **2004**, *39*, 1–8. [[CrossRef](#)]
36. Quang, T.N.; He, C.; Morawska, L.; Knibbs, L.D. Influence of ventilation and filtration on indoor particle concentrations in urban office buildings. *Atmos. Environ.* **2013**, *79*, 41–52. [[CrossRef](#)]
37. Kopperud, R.J.; Ferro, A.R.; Hildemann, L.M. Outdoor versus indoor contributions to indoor particulate matter (PM) determined by mass balance methods. *J. Air Waste Manag. Assoc.* **2004**, *54*, 1188–1196. [[CrossRef](#)] [[PubMed](#)]
38. Zhao, L.; Chen, C.; Wang, P.; Chen, Z.; Cao, S.; Wang, Q.; Xie, G.; Wan, Y.; Wang, Y.; Lu, B. Influence of atmospheric fine particulate matter (PM<sub>2.5</sub>) pollution on indoor environment during winter in Beijing. *Build. Environ.* **2015**, *87*, 283–291. [[CrossRef](#)]
39. Hussein, T. Indoor-to-outdoor relationship of aerosol particles inside a naturally ventilated apartment-A comparison between single-parameter analysis and indoor aerosol model simulation. *Sci. Total Environ.* **2017**, *596*, 321–330. [[CrossRef](#)] [[PubMed](#)]
40. Bo, M.; Salizzoni, P.; Clerico, M.; Buccolieri, R. Assessment of Indoor-Outdoor Particulate Matter Air Pollution: A Review. *Atmosphere* **2017**, *8*, 136. [[CrossRef](#)]
41. Hong, B.; Lin, B.; Qin, H. Numerical investigation on the coupled effects of building-tree arrangements on fine particulate matter (PM<sub>2.5</sub>) dispersion in housing blocks. *Sustain. Cities Soc.* **2017**, *34*, 358–370. [[CrossRef](#)]
42. Building Energy Conservation Research Center, Tsinghua University (BECRC). *Annual Report on Chinese Building Energy Conservation Development 2016*; China Architecture & Building Press: Beijing, China, 2016.
43. Shi, S.; Zhao, B. Occupants' interactions with windows in 8 residential apartments in Beijing and Nanjing, China. *Build. Simul.* **2016**, *9*, 221–231. [[CrossRef](#)]
44. Ye, B.; Ji, X.; Yang, H.; Yao, X.; Chan, C.K.; Cadle, S.H.; Chan, T.; Mulawa, P.A. Concentration and chemical composition of PM<sub>2.5</sub> in Shanghai for a 1-year period. *Atmos. Environ.* **2003**, *37*, 499–510. [[CrossRef](#)]
45. Beijing Municipal Environmental Monitoring Center (BMEMC). Real-Time Air Quality in Beijing. Available online: <http://www.bjmenc.com.cn> (accessed on 1 January 2016).
46. World Health Organization (WHO). WHO Air Quality Guidelines for Particulate Matter, Ozone, Nitrogen Dioxide and Sulfur Dioxide. Available online: [http://apps.who.int/iris/bitstream/10665/69477/1/WHO\\_SDE\\_PHE\\_OEH\\_06.02\\_eng.pdf](http://apps.who.int/iris/bitstream/10665/69477/1/WHO_SDE_PHE_OEH_06.02_eng.pdf) (accessed on 2 June 2005).
47. Freer-Smith, P.H.; Beckett, K.P.; Taylor, G. Deposition velocities to *Sorbus aria*, *Acer campestre*, *Populus deltoids* × *trichocarpa* 'Beaupré', *Pinus nigra* and × *Cupressocyparis leylandii* for coarse, fine and ultra-fine particles in the urban environment. *Environ. Pollut.* **2005**, *133*, 157–167. [[CrossRef](#)] [[PubMed](#)]
48. Franke, J.; Hellsten, A.; Schlunzen, K.H.; Carissimo, B. The COST 732 best practice guideline for CFD simulation of flows in the urban environment: A summary. *Int. J. Environ. Pollut.* **2011**, *44*, 419–427. [[CrossRef](#)]
49. Lin, B.; Li, X.; Zhu, Y.; Qin, Y. Numerical simulation studies of the different vegetation patterns' effects on outdoor pedestrian thermal comfort. *J. Wind Eng. Ind. Aerodyn.* **2008**, *96*, 1707–1718. [[CrossRef](#)]
50. Finnigan, J. Turbulence in plant canopies. *Annu. Rev. Fluid Mech.* **2000**, *32*, 519–571. [[CrossRef](#)]

51. Sanz, C. A note on k-epsilon modelling of vegetation canopy air-flows. *Bound.-Layer Meteorol.* **2003**, *108*, 191–197. [[CrossRef](#)]
52. Katul, G.G.; Mahrt, L.; Poggi, D.; Sanz, C. One-and two-equation models for canopy turbulence. *Bound.-Layer Meteorol.* **2004**, *113*, 81–109. [[CrossRef](#)]
53. Endalew, A.M.; Hertog, M.; Delele, M.A.; Baetens, K.; Persoons, T.; Baelmans, M.; Ramon, H.; Nicolai, B.M.; Verboven, P. CFD modelling and wind tunnel validation of airflow through plant canopies using 3D canopy architecture. *Int. J. Heat Fluid Flow* **2009**, *30*, 356–368. [[CrossRef](#)]
54. Ji, W.; Zhao, B. Numerical study of the effects of trees on outdoor particle concentration distributions. *Build. Simul.* **2014**, *7*, 417–427. [[CrossRef](#)]
55. Vranckx, S.; Vos, P.; Maiheu, B.; Janssen, S. Impact of trees on pollutant dispersion in street canyons: A numerical study of the annual average effects in Antwerp, Belgium. *Sci. Total Environ.* **2015**, *532*, 474–483. [[CrossRef](#)] [[PubMed](#)]
56. Jeanjean, A.P.R.; Monks, P.S.; Leigh, R.J. Modelling the effectiveness of urban trees and grass on PM<sub>2.5</sub> reduction via dispersion and deposition at a city scale. *Atmos. Environ.* **2016**, *147*, 1–10. [[CrossRef](#)]
57. Santiago, J.L.; Martilli, A.; Martin, F. On dry deposition modelling of atmospheric pollutants on vegetation at the microscale: Application to the impact of street vegetation on air quality. *Bound.-Layer Meteorol.* **2016**, *162*, 1–24. [[CrossRef](#)]
58. Bell, J.N.B.; Treshow, M. (Eds.) *Air Pollution and Plant Life*, 2nd ed.; John Wiley & Sons Ltd.: Chichester, UK, 2003.
59. Concentration Data of Street Canyons (CODASC). Available online: <http://www.windforschung.de/CODASC.htm> (accessed on 1 January 2008).
60. Gromke, C.; Blocken, B. Influence of avenue-trees on air quality at the urban neighborhood scale. Part I: Quality assurance studies and turbulent Schmidt number analysis for RANS CFD simulations. *Environ. Pollut.* **2015**, *196*, 214–223. [[CrossRef](#)] [[PubMed](#)]
61. Roache, P.J. Perspective: A method for uniform reporting of grid refinement studies. *J. Fluids Eng.* **1994**, *116*, 405–413. [[CrossRef](#)]
62. Gromke, C.; Ruck, B. Pollutant concentrations in street canyons of different aspect ratio with avenues of trees for various wind directions. *Bound.-Layer Meteorol.* **2012**, *144*, 41–64. [[CrossRef](#)]
63. Hanna, S.; Chang, J. Acceptance criteria for urban dispersion model evaluation. *Meteorol. Atmos. Phys.* **2012**, *116*, 133–146. [[CrossRef](#)]
64. Hong, B.; Lin, B.; Qin, H. Numerical investigation on the effect of avenue trees on PM<sub>2.5</sub> dispersion in urban street canyons. *Atmosphere* **2017**, *8*, 129. [[CrossRef](#)]
65. Hefny, M.M.; Ooka, R. CFD analysis of pollutant dispersion around buildings: Effect of cell geometry. *Build. Environ.* **2009**, *44*, 1699–1706. [[CrossRef](#)]
66. Barratt, R. *Atmospheric Dispersion Modeling: An Introduction to Practical Applications*; Earthscan: London, UK, 2001.
67. Jin, R.; Hang, J.; Liu, S.; Wei, J.; Liu, Y.; Xie, J.; Sandberg, M. Numerical investigation of wind-driven natural ventilation performance in a multi-storey hospital by coupling indoor and outdoor airflow. *Indoor Built Environ.* **2016**, *25*, 1226–1247. [[CrossRef](#)]
68. Lee, B.H.; Yee, S.W.; Kang, D.H.; Yeo, M.S.; Kim, K.W. Multi-zone simulation of outdoor particle penetration and transport in a multi-storey building. *Build. Simul.* **2017**, *10*, 525–534. [[CrossRef](#)]
69. King, M.; Gough, H.L.; Halios, C.; Barlow, J.F.; Robertson, A.; Hoxey, R.; Noakes, C.J. Investigating the influence of neighbouring structures on natural ventilation potential of a full-scale cubical building using time-dependent CFD. *J. Wind Eng. Ind. Aerodyn.* **2017**, *169*, 265–279. [[CrossRef](#)]
70. Chan, A.T. Indoor-outdoor relationships of particulate matter and nitrogen oxides under different outdoor meteorological conditions. *Atmos. Environ.* **2002**, *36*, 1543–1551. [[CrossRef](#)]

